Sepsis expands a CD39+ plasmablast population that promotes immunosuppression via adenosine-mediated inhibition of macrophage antimicrobial activity

Daniele Carvalho Nascimento, Paula Ramos Viacava, Raphael Gomes Ferreira, Marina Alves Damaceno, Annie Rocío Piñeros, Paulo Henrique Melo, Paula Barbim Donate, Juliana Escher Toller-Kawahisa, Daniel Zoppi, Flávio Protásio Veras, et al.

Sepsis expands a CD39+ plasmablast population that promotes immunosuppression via adenosine-mediated inhibition of macrophage antimicrobial activity

Daniele Carvalho Nascimento[1,2,3], Paula Ramos Viacava[1,2], Raphael Gomes Ferreira[1,2], Marina Alves Damaceno[4], Annie Rocío Piñeros[1,2], Paulo Henrique Melo[1,2], Paula Barbim Donate[1,2], Juliana Escher Toller-Kawahisa[1,2], Daniel Zoppi[5], Flávio Protásio Veras[1,2], Raphael Sanches Peres[1,2], Luísa Menezes-Silva[6], Diego Caetité[1,2], Antonio Edson Rocha Oliveira[7], Ícaro Maia Santos de Castro[7], Gilles Kauffenstein[8], Helder Imoto Nakaya[7], Marcos Carvalho Borges[5], Dario Simões Zamboni[2,9], Denise Morais da Fonseca[6], Jonas Augusto Rizzato Paschoal[4], Thiago Mattar Cunha[1,2], Valerie Quesniaux[3,10], Joel Linden[11], Fernando Queíroz Cunha[1,2], Bernhard Ryffel[3,10] and José Carlos Alves-Filho[1,2]

Affiliations

[1]Departments of Pharmacology, Ribeirão Preto Medical School, University of São Paulo, Ribeirão Preto, SP, 14049-900, Brazil;

[2]Center for Research in Inflammatory Diseases, Ribeirão Preto Medical School, University of São Paulo, Ribeirão Preto, SP, 14049-900, Brazil;

[3]CNRS, UMR7355, Orleans, 45071, France;

[4]Department of Biomolecular Sciences, School of Pharmaceutical Sciences of Ribeirão Preto, University of São Paulo, Ribeirão Preto, SP, 14049-900, Brazil;

[5]Department of Internal Medicine, Ribeirão Preto Medical School, University of São Paulo, Ribeirão Preto, SP, 14049-900, Brazil.

[6]ICB – Institute of Biomedical Sciences, University of São Paulo, São Paulo, SP, 05508-000, Brazil;

[7]Department of Clinical and Toxicological Analyses, School of Pharmaceutical Sciences, University of São Paulo, São Paulo, SP, 05508-000, Brazil;

[8]UMR INSERM 1260, Regenerative NanoMedicine, University of Strasbourg, Strasbourg, 60026, France;

[9]Department of Cell Biology, Ribeirão Preto Medical School, University of São Paulo, Ribeirão Preto, SP, 14049-900, Brazil;

[10]Experimental and Molecular Immunology and Neurogenetics, University of Orleans, Orleans, 45071, France;

[11]Division of Nephrology, Center for Immunity, Inflammation and Regenerative Medicine University of Virginia School of Medicine, Charlottesville, VA 22903, USA.

Corresponding authors

Daniele Carvalho Nascimento

danielecbn@usp.br

José Carlos Alves-Filho

jcafilho@usp.br

Lead contact

José Carlos Alves-Filho

jcafilho@usp.br

Keywords: Sepsis, adenosine, immunosuppression, B cells, plasmablast, macrophages.

Abstract

Sepsis results in elevated adenosine in circulation. Extracellular adenosine triggers immunosuppressive signaling via the A2a receptor (A2aR). Sepsis survivors develop persistent immunosuppression with increased risk of recurrent infections. We utilized the cecal ligation and puncture (CLP) model of sepsis and subsequent infection to assess the role of adenosine in post-sepsis immune suppression. A2aR-deficient mice showed improved resistance to post-sepsis infections. Sepsis expanded a subset of $CD39^{hi}$ B cells and elevated extracellular adenosine, which was absent in mice lacking CD39-expressing B cells. Sepsis-surviving B cell-deficient mice were more resistant to secondary infections. Mechanistically, metabolic reprogramming of septic B cells increased production of ATP, which was converted into adenosine by CD39 on plasmablasts. Adenosine signalling via A2aR impaired macrophage bactericidal activity and enhanced interleukin-10 production. Septic patients exhibited expanded $CD39^{hi}$ plasmablasts and adenosine accumulation. Our study reveals $CD39^{hi}$ plasmablasts and adenosine as important drivers of sepsis-induced immunosuppression, with relevance in human disease.

INTRODUCTION

Sepsis is a systemic inflammation triggered by pathogens that leads to organ dysfunction (Singer et al., 2016). Although advances in supportive care have reduced sepsis mortality over the last decades (Prescott and Angus, 2018), patients who survive severe sepsis have a high number of re-hospitalizations and increased mortality mainly due to recurrent infections (Otto et al., 2011; Wang et al., 2014). Compelling clinical and experimental studies indicate that sepsis may cause an immunosuppressive state that accounts for increased susceptibility to secondary, mostly opportunistic, infections (Benjamim et al., 2003; Boomer et al., 2011; Nascimento et al., 2017; Otto et al., 2011). Potential mechanisms for sepsis-induced immunosuppression include immune cell apoptosis, expansion of the regulatory T (Treg) cell population, and impaired microbial killing by macrophages (Mφs) (Venet and Monneret, 2018). However, the mechanisms underlying the persistent dysregulation of the host immune response in sepsis survivors are not entirely understood.

Extracellular adenosine is a signaling molecule that modulates several immunological processes via specific receptors expressed on immune cells (Hasko et al., 2008). Adenosine binds four different receptors: adenosine receptor 1 (A1R), A2aR, A2bR, and A3R (Fredholm et al., 2001). The signaling mediated by A2aR augments the production of anti-inflammatory cytokines, inhibits T cell proliferation, suppresses microbial killing by neutrophils and Mφs, and enhances differentiation of M2 Mφs (Hasko et al., 2008; Haskó and Cronstein, 2013).

A major source of extracellular adenosine is ATP hydrolysis by ectonucleotidases, such as CD39 and CD73 (Allard et al., 2017). CD39 (ectonucleoside triphosphate diphosphohydrolase-1, ENTPD1) catalyzes the hydrolysis of extracellular ATP and ADP to AMP, while CD73 (ecto-5′ nucleotidase, E5NT) converts AMP into adenosine (Colgan et al., 2006; Dwyer et al., 2007). During the acute phase of sepsis, patients show elevated adenosine levels in circulation (Jabs et al., 1998; Martin et al., 2000; Ramakers et al., 2011). We, therefore, hypothesized that increased extracellular adenosine might contribute to the development of immune suppression in sepsis survivors via activation of A2aR in immune cells.

Here, we showed that sepsis induced the expansion of splenic $CD39^{hi}CD138^{hi}$ plasmablasts, which generated increased extracellular adenosine in sepsis survivors. Adenosine derived from $CD39^{hi}CD138^{hi}$ plasmablasts promoted suppression of the immune response by impairing the microbicidal activity of macrophages via A2aR activation, rendering sepsis-surviving mice highly susceptible to secondary infections. Myeloid-specific deletion of A2aR improved the microbial resistance of sepsis-surviving mice. We found that septic patients also had an increased frequency of immunosuppressive $CD39^{hi}$ plasmablasts and adenosine accumulation in the blood. Our data, therefore, suggest that adenosine can be a potential therapeutic target for persistent immunosuppression in sepsis survivors.

RESULTS

Adenosine via A2aR mediates sepsis-induced immunosuppression

To investigate whether adenosine contributes to the development of immunosuppression after sepsis, we utilized cecal ligation and puncture (CLP; 100% lethality), a clinically relevant sepsis model (Nascimento et al., 2010; Rittirsch et al., 2009). Following CLP, mice received antibiotic treatment (ertapenem), which increased survival (60%; Figures 1A and 1B). Mice that survived were then challenged at day 15 post-CLP with an intranasal (i.n.) sub-lethal dose of one of two opportunistic human pathogens, *L. pneumophil*a or *A. fumigatus*, to examine host susceptibility to secondary infections (Figure 1A). As previously described (Nascimento et al., 2017), sepsis-surviving mice showed impaired microbial clearance and high susceptibility to both infections (100% and 80% lethality, respectively), while all naive or sham-operated immune-competent mice survived until the end of the study period (Figures 1C-1F and Figure S1A). The high susceptibility of sepsis-surviving mice to challenge infection with *L. pneumophila* persisted for at least 75 days post-CLP (Figure 1C). Mice that survived moderate CLP model with or without antibiotics (70% and 20% lethality, respectively) were equally susceptible to the challenge infection with *L. pneumophila* (Figures S1B and S1C). We then measured adenosine concentration in the plasma at different time points after sepsis induction (Figure 1G). Circulating adenosine increased in sepsis-surviving mice by day 15, which peaked around day 45 and remained elevated above naïve and sham-operated mice out to day 75 (Figures 1H and 1I, Figures S1D and S1E and Figure S2I).

To investigate whether the A2aR contributes to immunosuppression, we treated CLP mice with A2aR antagonist (A2aRi; 8-3-chlorostyryl-caffeine) (Jacobson et al., 1993) and challenged sepsis-surviving mice with *A. fumigatus* or *L. pneumophila* 15 days post-CLP (Figure 1J). A2aR blockade enhanced host resistance against both infections (Figure 1K) and reduced microbial loads in the lungs and spleen of sepsis-surviving mice (Figure 1L). Sepsis-surviving A2aR-deficient (*Adora2a*$^{-/-}$) mice also showed lower *L. pneumophila* counts in the lung and spleen than BALB/c WT mice (Figure 1M). The inhibition or deficiency of A2aR did not alter the survival of antibiotic-treated CLP mice (Figures S2A-S2C). Thus, adenosine signaling via the A2aR is required for the development of sepsis-induced immunosuppression.

Adenosine accumulation in sepsis-surviving mice requires CD39 activity

Because the hydrolysis of extracellular ATP by CD39 is considered the primary source of extracellular adenosine (Robson et al., 2006), we next asked whether CD39 contributes to post-sepsis immunosuppression. Flow cytometry analysis revealed increased CD39 expression in spleen cells from sepsis-surviving mice 15 days post-CLP (Figure 2A). We then incubated spleen cells with ATP and measured inorganic phosphate (Pi) released in the cell supernatants to analyze ecto-ATPase activity. Spleen cells from sepsis-surviving mice showed elevated ecto-ATPase activity 15 days post-CLP compared to naive mice (Figure 2B). This was reduced by pre-incubation with CD39 inhibitor, ARL 67156 (CD39i) (Lévesque et al., 2007). These data suggest that CD39 activity is important for the hydrolysis of ATP by splenic cells from CLP mice.

To investigate whether CD39 is required for the increased circulating adenosine, we induced CLP in CD39-deficient (*Entpd1*$^{-/-}$) mice or treated C57BL/6 WT mice with CD39i (Figure 2C). Both approaches abolished plasma adenosine accumulation in sepsis-surviving mice (Figures 2D-2F). Moreover, CD39 inhibition improved survival rates of sepsis-surviving mice challenged with *A. fumigatus* or *L. pneumophila* 15 days after CLP (Figure 2G). *L. pneumophila* counts were reduced in the lungs and spleen of mice treated with CD39i compared to vehicle-treated mice (Figure 2H). Similarly, sepsis-surviving *Entpd1*$^{-/-}$ mice showed lower fungal burdens in the lungs and a higher survival rate to *A. fumigatus* infection than WT control mice (Figures 2I and 2J). Loss of CD39 did not alter the survival of antibiotic-treated CLP mice (Figures S2D and S2E). These results indicate that CD39 is critical for the production of extracellular adenosine and sepsis-induced immunosuppression development.

Sepsis promotes the expansion of a CD39-expressing B cell population

CD39 is expressed on many immune cell types (Antonioli et al., 2013; Dwyer et al., 2007). To gain an unbiased perspective on the CD39 expression pattern in immune cells from sepsis-surviving mice, we performed high-dimensional flow cytometric analyses of the splenic CD39^{+} cell populations of naïve and sepsis-surviving mice. We used the t-distributed stochastic neighbor embedding (t-SNE) algorithm to perform an unsupervised analysis of the entire flow cytometry dataset (10 samples) generated from naïve and sepsis-surviving mice. Representative t-SNE maps color-coded according to cluster annotation for immune cell populations. Expression intensity revealed that most immune cell populations express CD39 in both naive and sepsis-surviving mice 15 days after

CLP (Figures 3A and 3B and Figures S3A and S3B). However, the frequency of $CD39^+$ B cells and the levels of CD39 expression in B cells were particularly increased in sepsis-surviving mice compared to other immune cell populations and B cells from naïve mice (Figure 3C and Figure S3B). Moreover, a small population of $CD39^{hi}$ B cells was enriched in the spleens of sepsis survivors (Figures 3B and 3C and Figure S3B). CD39 expression was also increased in B cells from the blood but not from peripheral lymph nodes (LNs) of sepsis-surviving mice (Figures S3C and S3D). Compared with naïve mice, an increased proportion of $CD39^{hi}$ splenic B cells from sepsis-surviving mice co-expressed the proliferation marker Ki67 (Gerdes et al., 1984), suggesting that sepsis leads to an expansion of a $CD39^{hi}$ B cell population (Figure 3D). Sham and naive mice ± antibiotics showed a lower frequency of splenic $CD39^+$ B cells than sepsis-surviving mice 15 days after CLP (Figure S1F).

To characterize B cell subsets expressing CD39, a separate high-dimensional flow cytometric analysis was performed. We enriched $CD45^+CD19^+$ B cell populations from spleens by negatively selecting against the T and Treg cell markers CD3 and Foxp3. We then identified various $CD19^+$ B cell subsets based on traditional flow cytometry gating strategies, as described (Culton et al., 2006; Tung et al., 2006): pre-B ($CD138^-IgM^-IgD^-$), immature B ($CD138^-IgM^+IgD^-$), early-($CD138^-IgM^+IgD^+$) and late-mature B ($CD138^-IgM^-IgD^+$) and plasmablast ($CD138^{hi}$) cells (Figure S3E). Representative t-SNE maps color-coded according to cluster annotation for distinct $CD39^+$ B cell subsets showed that CD39 is expressed in most splenic B cell populations in both naive and sepsis-surviving mice 15 days after CLP (Figure 3E). However, t-SNE heatmaps revealed that a

differentiated group of cells corresponding to $CD138^{hi}$ plasmablasts (orange) showed the highest CD39 expression in sepsis-surviving mice (Figures 3F and 3G). To extend the analysis of CD39 expression on B cell subsets in sepsis-surviving mice, we performed a time-course experiment to profile CD39 expression on B1a ($CD138^{-}CD5^{+}CD23^{-}$), B1b ($CD138^{-}CD5^{-}CD23^{-}$), and B2 ($CD138^{-}CD5^{-}CD23^{+}$) and plasmablast ($CD138^{hi}$) cells in the spleen of mice after CLP induction (Figure 3H). We confirmed that plasmablasts expressed higher levels of CD39 than other B cell subsets, including B1a, B1b, and B2 cells (Figure 3I). Besides, B1a and B1b cells from sepsis-surviving mice had increased expression and frequency of CD39, while these parameters were not altered in B2 cells (Figures 3I-3K). The frequency and the absolute number of $CD39^{+}CD138^{hi}$ B cells increased in sepsis-surviving mice, peaking on day 7 and returning to baseline levels within 75 days after CLP, indicating that sepsis leads to the expansion of $CD39^{+}CD138^{hi}$ B cells (Figures 3J-3M). In support of this, the frequency and number of $Ki67^{+}CD39^{+}CD138^{hi}$ B cells were increased in sepsis-surviving mice (Figures 3J and 3N-3P). Finally, to address which splenic B cell compartment $CD39^{hi}$ B cells reside, we performed flow cytometry analysis of splenic cells from sepsis-surviving mice on day 7 after CLP, including additional surface markers to characterize marginal zone (MZ) ($B220^{+}IgM^{+}CD21^{hi}CD23^{lo}$), follicular (FO) ($B220^{+}IgM^{+}CD21^{int}CD23^{hi}$), and immature transitional T1 B cells ($B220^{+}IgM^{+}CD21^{-}CD23^{-}$) (Figure S4A). $CD39^{hi}$ B cells were characterized in immature transitional T1 cells, co-expressing $CD138^{hi}$ (Figures S4B and S4C). Thus, sepsis induces the expansion of a $CD39^{hi}CD138^{hi}$ plasmablast population.

$CD39^{+}$ B cells are critical for sepsis-induced immunosuppression

Our results led us to ask whether B cells contribute to extracellular adenosine production and, consequently, immunosuppression after sepsis. $CD19^+$ B cells sorted from the spleens of sepsis-surviving mice at day 15 post-CLP had increased mRNA levels of *Entpd1* (encoding CD39) (Figure 4A). We then assessed ATPase activity and the ability of B cells to generate adenosine through ATP hydrolysis. Upon addition of exogenous ATP, B cells from sepsis-surviving mice showed higher ecto-ATPase activity and produced more adenosine than naive B cells, which was abolished by CD39i (Figure 4B and 4C). Next, we measured plasma adenosine concentrations in *Rag1*$^{-/-}$ mice, which lack mature T- and B-lymphocytes. Sepsis-surviving *Rag1*$^{-/-}$ mice showed lower plasma adenosine concentration than WT mice at 15 days post-CLP. Adoptive transfer of naive $CD19^+$ B cells into *Rag1*$^{-/-}$ recipient mice before CLP induction increased the systemic concentration of adenosine to levels comparable to those observed in septic WT mice (Figures 4D-4F and Figure S2K). Nearly all transferred $CD138^{hi}$ B cells expressed CD39, and the $Ki67^+$ proportion was comparable between B cell-recipient *Rag1*$^{-/-}$ and WT mice. The absolute number of $CD39^+$ B cells in sepsis-surviving *Rag1*$^{-/-}$ mice transferred with B cells was lower than WT mice but significantly higher compared to naive WT mice (Figure 4G). Consistently, spleen cells from μMT$^{-/-}$ mice, which lack mature peripheral B cells, showed low ecto-ATPase activity, and mice failed to raise plasma concentration of adenosine 15 days after CLP (Figures 4H-4J and Figure S2J). Sepsis-surviving μMT$^{-/-}$ mice were more resistant to *L. pneumophila* infection at day 15 post-CLP, showing higher survival rate and lower bacterial loads in the lungs and spleen than WT mice (Figures 4K and 4L). There was no difference in CLP survival between *Rag1*$^{-/-}$, μMT$^{-/-}$, and WT mice under antibiotic treatment (Figures S2F and S2G).

We then investigated whether the absence of CD39 in B cells would reduce adenosine accumulation in sepsis-surviving mice. To this end, we generated mixed bone marrow (BM) chimeras whereby irradiated WT mice were reconstituted with a mixture of 80 % μMT$^{-/-}$ BM cells and either 20% WT (WT μMT-chimera) or 20 % *Entpd1*$^{-/-}$ (*Entpd1*$^{-/-}$ μMT-chimera) BM cells (Figure 4M). Reconstitution was assessed eight weeks after adoptive transfer (Figures S4D and S4E). With this experimental approach, reconstituted *Entpd1*$^{-/-}$ μMT-chimeric mice harbored *Entpd1*$^{-/-}$ B cells in an environment of mostly WT cells. Splenic B cells from WT μMT-chimeras showed increased expression of CD39 after CLP compared to naïve mice. In contrast, CD39 expression was reduced in B cells from *Entpd1*$^{-/-}$ μMT-chimeric mice from both naïve and CLP groups (Figure 4N). Spleen cells from *Entpd1*$^{-/-}$ μMT-chimeric mice showed low ecto-ATPase activity, and mice failed to increase blood adenosine concentration 15 days after CLP (Figures 4O and 4P and Figure S2L). Since Mφs from sepsis-surviving mice have impaired bactericidal ability (Nascimento et al., 2017), we asked whether the lack of CD39 on B cells would prevent the reduction of bactericidal ability. To this end, peritoneal Mφs isolated from sepsis-surviving WT and *Entpd1*$^{-/-}$ μMT-chimeric mice were cultured and infected with *L. pneumophila,* and the number of viable intracellular bacteria was assessed (Figure 4Q). The impaired bactericidal activity found in Mφs from WT μMT-chimeric mice was not observed in Mφs from *Entpd1*$^{-/-}$ μMT-chimeric mice (Figure 4R). Finally, we investigated whether septic B cells would directly affect host resistance to infection by transferring sorted CD19^{+} B cells from naive or sepsis-surviving mice 15 days post-CLP into naive WT mice. Seven days later, we challenged mice with *L. pneumophila* i.n. (Figure S5A). Mice

receiving septic B cells showed higher bacteria burdens in the lung than those receiving naive B cells or no B cells, suggesting that septic B cells suppress infection control (Figure S5B). Altogether, our data suggest that $CD39^+$ B cells play a central role in producing adenosine and suppressing the immune response in sepsis survivors.

B cell-derived adenosine impairs microbial killing in Mφs *in vitro*

To investigate *in vitro* how septic B cells suppress immune responses to infection, peritoneal Mφs from naive mice were infected with *L. pneumophila* and co-cultured with B cells isolated from naive or sepsis-surviving mice for 48 h (Figure 5A). Naive B cells did not affect the ability of Mφs to restrict bacterial replication. However, Mφs co-cultured with septic B cells contained significantly more bacteria than Mφs co-cultured with naïve B cells or Mφs alone (Figure 5B). Naïve or septic B cells did not harbor any intracellular bacteria after 48 h of culture.

The immunomodulatory effects of adenosine include enhanced IL-10 production (Haskó and Pacher, 2012). IL-10 can compromise host defence by directly inhibiting microbial killing by Mφs (Couper et al., 2008). IL-10 plays a critical role in the sepsis-induced impairment of lung host defence to secondary infections (Nascimento et al., 2017; Steinhauser et al., 1999). IL-10 production by *L. pneumophila*-infected Mφs was enhanced after 48 h of co-culture with septic B cells, but not naïve B cells (Figure 5C). Naïve or septic B cells alone released minor levels of IL-10 in response to *L. pneumophila* infection (Figure 5C). *Il10*$^{-/-}$ Mφs exhibited improved killing compared with WT Mφs, and septic B cells failed

to suppress bacterial killing in *Il10*$^{-/-}$ Mφs (Figure 5D). Thus, IL-10 produced by Mφs is critical for the suppressive effect of septic B cells.

We next sought to explore how septic B cells suppress Mφ bacterial killing. Mφs treated with CD39i and co-cultured with septic B cells showed enhanced restriction of *L. pneumophila* replication, similar to levels observed with Mφs co-cultured with naïve B cells or Mφs alone (Figure 5E). In contrast, the addition of apyrase, a soluble ATPase, in the culture, impaired the restriction of bacterial replication by Mφs co-cultured with septic B cells and also with naïve B cells, to a lesser extent (Figure 5E). Supplementation of cultures with ATPγS, a non-hydrolyzable ATP analog, did not affect bacterial killing by Mφs alone or in co-culture with B cells. Conversely, adenosine deaminase (ADA), an adenosine-degrading enzyme, abrogated the suppressive effect of septic B cells on Mφ bacterial killing (Figure 5E). Collectively, these data suggest that the hydrolysis of ATP into adenosine is required for the suppression of Mφ bacterial killing by septic B cells.

Next, *Entpd1*$^{-/-}$ Mφs or B cells were co-cultured to examine the relative contribution of CD39 on these cells to suppress microbial killing. *Entpd1*$^{-/-}$ Mφs co-cultured with septic WT B cells showed bacterial viability similar to that observed with WT Mφs (Figure S5C). In contrast, reduced bacterial viability was seen with CD39 deficiency in septic B cells alone or in both Mφs, suggesting restored bacterial killing (Figure 5F and Figure S5C). The addition of apyrase impaired bacterial killing in Mφs co-cultured with *Entpd1*$^{-/-}$ septic B cells (Figure 5F). CD39^{+} B cells sorted from both naive or septic-surviving mice strongly

suppressed bacterial killing by Mφs, while $CD39^-$ septic B cells showed a weak suppressive effect (Figure 5G). Thus, CD39-expressing septic B cells suppress Mφ bacterial killing through adenosine production.

Next, we investigated the effect of adenosine on Mφ microbial killing. A2aRi treatment improved bacterial killing, especially in co-culture with septic B cells (Figure S5D). However, A2bR blockade (A2bRi) did not affect the bactericidal activity of Mφs alone or in co-culture with B cells (Figure S5E). Peritoneal Mφs from mice lacking A2aR in myeloid cells (*Adora2a*$^{\Delta Lyz2}$) limited intracellular bacterial infection more efficiently than WT (*Adora2a*$^{f/f}$) Mφs. Moreover, septic B cells failed to suppress bacterial killing by *Adora2a*$^{\Delta Lyz2}$ Mφs (Figure 5H). Taken together, these data support the hypothesis that adenosine derived from $CD39^+$ B cells suppresses the immune response after sepsis, at least in part, through suppression of Mφ microbial killing.

We then investigated whether B cell-derived adenosine induces IL-10 production in Mφs. Although septic B cells enhanced Mφ production of IL-10 in response to *L. pneumophila* infection, the addition of CD39i or ADA to the co-cultures completely abrogated this effect, while ATPγS did not alter IL-10 levels (Figure 5I). Moreover, *Entpd1*$^{-/-}$ septic B cells failed to increase IL-10 production by *L. pneumophila*-infected Mφs (Figure 5J), suggesting that the hydrolysis of ATP into adenosine by $CD39^+$ B cells induces the production of IL-10 by *L. pneumophila*-infected Mφs. Loss or inhibition of A2aR in *L. pneumophila*-infected Mφs reduced their production of IL-10 when co-cultured with septic B cells, but also with naïve B cells or when cultured alone (Figures 5K and 5L). Overall, our findings

demonstrate that B cell-derived adenosine suppresses bacterial killing by inducing the production of IL-10 in Mφs.

To validate the relevance of our *in vitro* observations *in vivo*, we utilized IL-10$^{+/EGFP}$ reporter mice and found increased IL-10 expression by splenic Mφs from sepsis-surviving mice 15 days after CLP (Figure 5M). Moreover, sepsis-surviving mice show robust IL-10 in lung tissue homogenates, which was reduced with A2aRi or CD39i and in *Adora2a*$^{-/-}$ and μMT$^{-/-}$ mice (Figure S5F). Sham and naive mice had low levels of IL-10 in lung tissue homogenates (Figures S1G). Finally, to investigate the role of A2aR on Mφs in developing sepsis-induced immunosuppression, we induced CLP in *Adora2a*$^{\Delta Lyz2}$ mice. Sepsis-surviving *Adora2a*$^{\Delta Lyz2}$ mice were resistant to *L. pneumophila* challenge 15 days post-CLP, showing a lower number of *L. pneumophila* in the lung and spleen and reduced IL-10 in lung tissue homogenates than control mice (Figures 5N-5P). There was no difference in CLP survival between *Adora2a*$^{\Delta Lyz2}$ or control mice with antibiotic treatment (Figure S2H). Together, these data indicate that A2aR signaling on Mφs is required for IL-10 production and, consequently, for the immune dysfunction in sepsis-surviving mice.

Metabolic reprogramming in septic B cells supports their suppressive function

Given that septic B cells suppress Mφ-mediated bacterial killing through ATP hydrolysis into adenosine, we hypothesized a role for B cell metabolic reprogramming induced by sepsis. To explore this possibility, we initially assessed the extracellular acidification rate (ECAR) and oxygen consumption

rate (OCR) in isolated $CD19^+$ B cells. Septic B cells showed higher ECAR and OCR than naive B cells, suggesting that septic B cells have increased glycolytic flux and mitochondrial activity. We then utilized inhibitors of the metabolic pathways required for ATP generation (Figure 6A). UK-5099, an inhibitor of the mitochondrial pyruvate transporter, reduced all respiratory parameters in septic B cells to similar levels found in naive B cells (Figures 6B-6E), demonstrating a critical dependence on glycolysis for the increased mitochondrial respiratory activity of septic B cells. Septic B cells had increased uptake of a fluorescent glucose analog (2-NBDG) and higher mRNA expression of glycolytic related genes *Hif1a* (hypoxia-inducible factor-1a), *Hk1* and *Hk2* (hexokinase-1 and 2, respectively), compared to naive B cells (Figures 6F and 6G). These data suggest that septic B cells are metabolically reprogrammed toward aerobic glycolysis that feeds the mitochondrial tricarboxylic acid (TCA) cycle.

We next investigated the impact of metabolic reprogramming of septic B cells on ATP production. Consistent with increased glycolytic flux and mitochondrial activity, unstimulated or IL-4-activated septic B cells contained more intracellular ATP than naive B cells. The addition of glycolytic inhibitors 2-deoxyglucose (2-DG), 3PO (PFKFB3 inhibitor), or echinomycin (HIF-1α inhibitor) reduced ATP production in septic B cells to similar levels found in naive B cells. Likewise, the addition of oligomycin (an inhibitor of mitochondrial ATP synthase) or rotenone (an inhibitor of mitochondrial complex I) decreased ATP production in septic B cells. However, ATP production in septic B cells was not affected by etomoxir (a carnitine palmitoyltransferase-1a inhibitor) or BPTES (a glutaminase-1 inhibitor). These results suggest that the enhanced mitochondrial activity and ATP

production in septic B cells require glycolytic activity, but not glutaminolysis or fatty acid oxidation (Figures 6H). We then investigated if the increased metabolic affected the extracellular release of ATP and found enhanced ATP release by septic B cells than naive B cells, which was abrogated by inhibiting the pannexin-1 ATP-permeable channel (Panx1) with CBX (Figures 6I and 6J).

Finally, to indirectly investigate the effect of metabolic reprogramming in sustaining septic B cells' suppressive activity, peritoneal Mφs from naive mice were infected with *L. pneumophila* and co-cultured with B cells isolated from naive or sepsis-surviving mice for 48 h with or without CBX. Panx1 inhibition by CBX did not directly affect bacterial killing by Mφs alone or in co-culture with naive B cells. However, the CBX abrogated the inhibitory effect of septic B cells on Mφ bacterial killing and reduced Mφs production of IL-10 (Figures 6K-6M). Collectively, our findings suggest that septic B cells have a metabolic reprogramming toward aerobic glycolysis that feeds mitochondrial TCA cycle, supporting their suppressive activity by enhancing production and release of ATP.

Septic patients have an expansion of CD39$^+$ plasmablast and adenosine accumulation

To investigate the clinical relevance of our findings, we collected peripheral blood samples from 21 septic patients and 36 age- and sex-matched healthy controls (HC). All patients presented clinical and laboratory variables that fulfilled sepsis criteria (Table S1). As observed in septic mice, the frequency of Ki67$^+$CD39$^+$CD19$^+$ B cells was increased in septic patients compared to HC

(Figure 7A). Naïve and memory B cells expressed intermediate levels of CD39 at comparable frequencies between septic patients and HC (Figures 7B and 7C). However, CD39 was highly expressed in plasmablasts, and septic patients showed a higher frequency than HC (Figures 7B-7D). Sorted $CD19^+$ B cells from septic patients showed increased ecto-ATPase activity compared to HC, which was inhibited by CD39i (Figure 7E). Inline, septic patients had higher plasma adenosine concentrations than HC (Figure 7F). Dividing septic patients by illness severity, adenosine levels were higher in patients with septic shock than sepsis only (Figure 7G), as previously reported (Martin et al., 2000). Moreover, the ecto-ATPase activity of isolated $CD19^+$ B cells positively correlated with serum adenosine concentration in septic patients (Figure 7H), suggesting that the elevated adenosine concentration was associated with CD39 activity in B cells.

To investigate whether human septic B cells could suppress monocytes' bacterial killing capacity, sorted $CD19^+$ B cells from 3 different septic patients or healthy volunteers were co-cultured with $CD14^+$ monocytes isolated from HC blood. We assessed bacterial load by using an *L. pneumophila* strain stably expressing the luxCDABE operon. Monocytes co-cultured with B cells from septic patients contained more bacteria than those co-cultured with B cells from healthy volunteers or monocytes alone. To address adenosine's contribution to bacterial killing suppression, we added A2aRi or apyrase in culture. A2aRi improved bacterial killing by monocytes, whereas apyrase impaired monocyte restriction of bacterial replication, especially when co-cultured with septic B cells (Figure 7I). *L. pneumophila*-driven IL-10 production by monocytes was enhanced by co-

culture with B cells from septic patients but not healthy volunteers. This was inhibited by A2aRi and further enhanced with the addition of apyrase (Figure 7J).

Finally, we analyzed publicly available single-cell RNA-seq data from PBMCs of septic patients and controls (Reyes et al., 2020). Gene expression analysis identified one distinct B cell population characterized by both high expression of CD39 and plasmablast markers (*MZB1*, *JCHAIN*, *FKBP11*, *SEC61G*, *VIMP*, *ITM2C*, *IGHA1*, and *TXN*). Similar to the CLP model, we found that septic patients had a greater abundance of $CD39^+$ plasmablast cells than the controls (no sepsis) (Figures 7K and 7L). Furthermore, differential expression analysis of $CD39^+$ plasmablast cells against other B cells revealed high expression of mitochondrial genes and enrichment of genes participating in the metabolic TCA cycle, respiratory electron transportation, detoxification of reactive oxygen species, and glycolysis (Figures S6A and S6B). Overall, these results substantiate our findings with experimental sepsis, showing an expansion of $CD39^+$ plasmablasts with immunosuppressive activity in septic patients.

DISCUSSION

Inflammatory environments can induce differentiation and/or expansion of distinct subsets of regulatory B cells that suppress pathological or protective immune responses (Rosser and Mauri, 2015). Activated B cells can express CD39 and, therefore, produce adenosine in the presence of extracellular ATP (Maliszewski et al., 1994; Saze et al., 2013). Similar to Treg cells, CD39 expression contributes to B cell suppressive function *in vitro* (Borsellino et al., 2007; Deaglio et al., 2007; Figueiró et al., 2016; Peres et al., 2015; Saze et al., 2013); however, the implications of this suppression remain underexplored. In this study, we report that sepsis induced an expansion of a plasmablast population in mice and human septic patients with elevated CD39 expression responsible for increasing circulating extracellular adenosine. Adenosine derived from CD39-expressing B cells suppressed the host immune response, rendering sepsis-surviving mice highly susceptible to secondary infections induced by opportunistic human pathogens, *A. fumigatus* and *L. pneumophila* (Behnsen et al., 2008; Berjeaud et al., 2016).

Adenosine signaling mediated by A2aR augments the production of anti-inflammatory cytokines and suppresses microbial killing by neutrophils and Mφs (Hasko et al., 2008; Haskó and Cronstein, 2013). Consistent with this, we found that septic B cell-derived adenosine efficiently suppressed Mφs killing ability and the specific deficiency of A2aR in myeloid cells improved the resistance of sepsis-surviving mice against secondary infections. These demonstrate the essential role of adenosine-producing B cells in developing sepsis-induced immunosuppression by suppressing macrophage function. However, an

unexpected finding was that IL-10, which has long been considered the central suppressive mediator produced by regulatory B cells (Rosser and Mauri, 2015), did not directly influence the suppressive activity of septic $CD39^+$ B cells. Instead, we found that Mφs respond to adenosine from CD39-expressing B cells via A2aR signaling by producing immunosuppressive IL-10 that impairs their bactericidal activity. Indeed, it was previously reported that, in the absence of IL-10, a CD39/CD73 pathway mediates the regulatory function of peritoneal B1 cells via the production of adenosine (Kaku et al., 2014). This was further supported by our observations that splenic B1a cells show a slight up-regulation of CD39 expression in sepsis-surviving mice. Thus, we cannot exclude the contribution of $CD39^{lo}$ B1a cells working together with $CD39^{hi}CD138^{hi}$ plasmablasts to the immunosuppressive status observed in sepsis-surviving mice.

We found that septic B cells have a metabolic reprogramming toward aerobic glycolysis that feeds mitochondrial TCA cycle with pyruvate enhancing production and release of ATP. These findings are consistent with previous reports of increased glycolysis and oxygen consumption rate by activated B cells with LPS or IL-4 (Caro-Maldonado et al., 2014; Waters et al., 2018). We, therefore, propose that the metabolic reprogramming in septic $CD39^+$ B cells supports their suppressive activity by enhancing the production and release of ATP.

In our study, antibiotic treatment of naive or sham-operated mice did not alter the frequency of CD39-expressing B cells and plasma adenosine concentration. Moreover, mice who survived to moderate sepsis receiving or not antibiotic treatment were equally susceptible to the secondary infection, suggesting that

antibiotic treatment does not directly impact sepsis-induced immune dysregulation. However, it is very complicated to dissociate the consequences of sepsis itself from the effect of sepsis treatment on the long-term immune dysregulation found in sepsis survivors since all septic patients inevitably receive antibiotic treatment. This is the reason why we have established a mouse model of lethal CLP-induced sepsis followed by a short treatment with ertapenem, a widely used antibiotic to treat critically ill patients with abdominal sepsis (Solomkin et al., 2010), intending to reduce infection and mimicking the clinical scenario (Nascimento et al., 2010). Future studies are required to determine whether the expansion of $CD39^+$ B cells reported here is due to inflammation following sepsis or a combination with changes in the microbiota by antibiotics.

IL-10 has long been described as a major mediator of sepsis-induced immunosuppression (Steinhauser et al., 1999). We have previously reported that IL-33, released during the tissue injury following sepsis, induces activation of ILC2s and the polarization of IL-10-secreting M2 macrophages that promote the expansion of the Treg cell population in an IL-10-dependent manner, thereby contributing to the development of sepsis-induced immunosuppression (Nascimento et al., 2017). However, our current understanding of the primary IL-10–secreting immune cells and the signaling that maintains IL-10 production in sepsis survivors remains limited. This study addressed this gap, revealing that adenosine-derived from $CD39^+$ B cells is an essential mediator that triggers IL-10 production by macrophages in sepsis-surviving mice, thus fitting the pieces of the intricate mechanism underlying the persistent dysregulation of the host immune response in sepsis survivors. However, we did not investigate the

mechanism by which sepsis induces the expansion of $CD39^+$ B cells. In this regard, IL-33 was shown to induce a subset of IL-10-producing regulatory B cells (Sattler et al., 2014). Based on our previous study (Nascimento et al., 2017), IL-33 might have a potential involvement, but we cannot exclude the participation of other cytokines or gut-microbiota-derived metabolites (Rosser et al., 2020; Yoshizaki et al., 2012). Therefore, future studies are necessary to identify the mechanism underlying the $CD39^+$ B cell expansion induced by sepsis.

In summary, our results revealed a suppressive function of $CD39^+$ plasmablasts that is responsible, at least in part, for the long-term immunosuppression observed in sepsis survivors by generating a high amount of extracellular adenosine. These findings fill gaps in the current knowledge of the mechanism underlying the persistent dysregulation of the host immune response in sepsis survivors.

LIMITATIONS OF THE STUDY

We demonstrated that the metabolic reprogramming in septic $CD39^+$ plasmablasts supports their suppressive activity by enhancing ATP production. However, extracellular ATP can be released by some bacteria from mouse and human feces (Mempin et al., 2013). Future studies are needed to determine whether perturbation of gut microbiota following sepsis might affect the systemic bioavailability of extracellular ATP and adenosine production by $CD39^+$ B cells. In addition, although we provided preliminary evidence showing that $CD39^{hi}CD138^{hi}$ B cells are enriched in the transitional 1 population, further

studies are needed to better characterize where exactly these cells reside in the spleen.

Acknowledgments

We thank Ieda Schivo, Sergio Rosa, Ana Katia Santos, Denise Ferraz and Marc Le Bert for technical assintances. This work was supported by Sao Paulo Research Foundation (FAPESP) grant (2013/08216-2 - Center for Research in Inflammatory Diseases), National Council for Scientific and Technological Development (CNPq) grant (483659/2013-4), FAPESP fellowships for D.C.N. (2012/10100-0 and 2015/25974-3) and European funding in Region Centre-Val de Loire grants (FEDER 2016-00110366, EX005756 and EUROFéRI EX010381).

Author Contributions

D.C.N. planned and performed experiments, analysed data and wrote the manuscript. J.C.A-F planned experiments, analyzed data, wrote the manuscript and supervised the project. B.R., F.Q.C., V.Q., and T.M.C. planned and analyzed experiments. P.R.V., R.G.F., A.R.P., P.H.M., P.B.D., F.P.V., R.S.P., J.E.T-K., D.C., M.A.D and J.A.R.P performed and analyzed experiments. D.Z. and M.C.B. provided human samples and analyzed data. L.M-S and D.M.F performed flow cytometry experiments and analyzed t-SNE data. A.E.R.O., Í.M.S.C., and H.I.N. re-analyzed public datasets. G.K. provided *Entpd1*$^{-/-}$ mice and analyzed data. J.L. provided *Adora2a*$^{f/f}$ mice and analyzed data. D.S.Z. provided reagents and analyzed data.

Competing Interests statement

The authors declare no competing interests.

Inclusion and diversity

We worked to ensure gender balance in the recruitment of human subjects. One or more of the authors of this paper self-identifies as an underrepresented ethnic minority in science. One or more of the authors of this paper self-identifies as a member of the LGBTQ+ community.

Figure 1

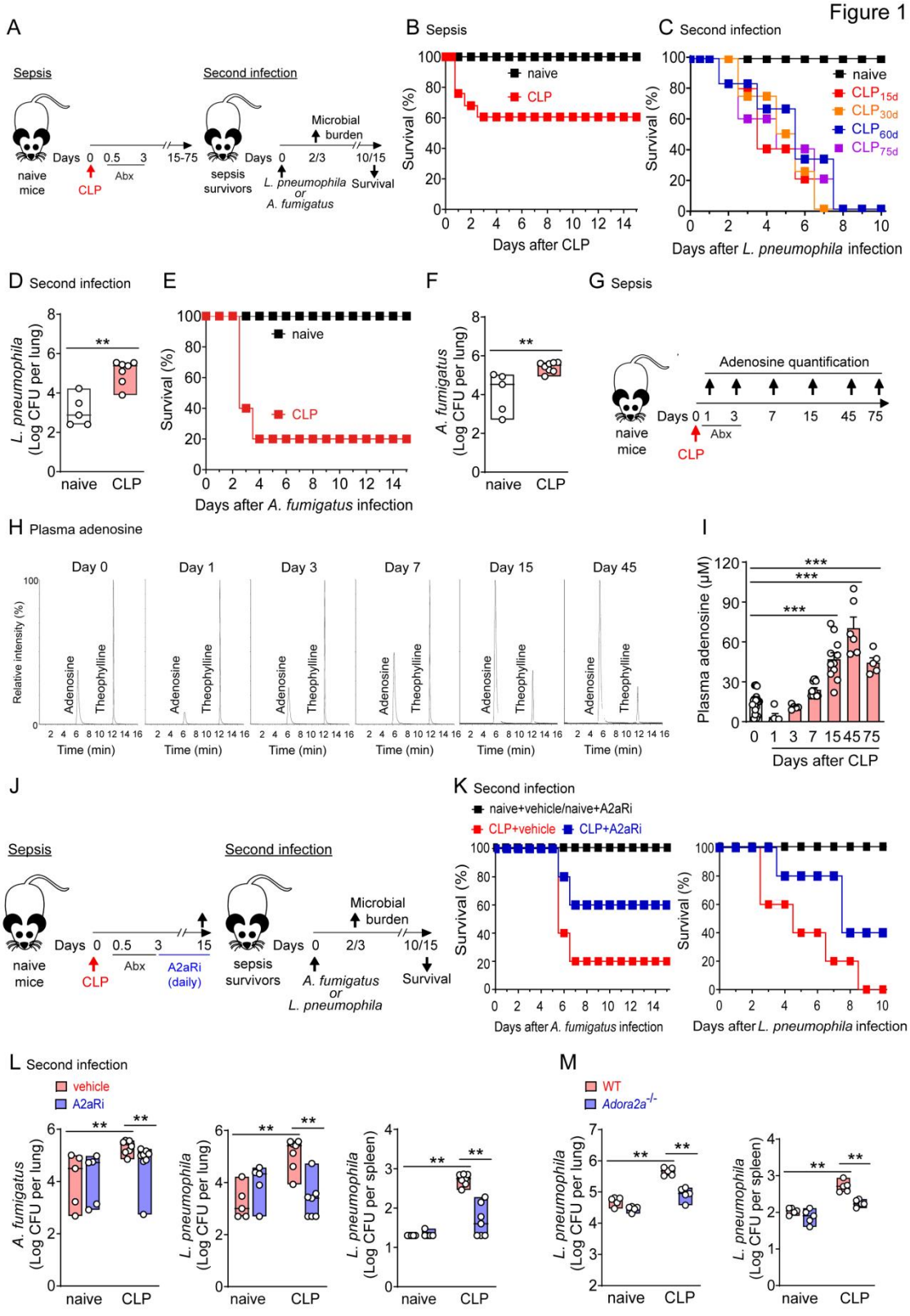
A
Sepsis
Second infection
naive mice
CLP
Days 0 0.5 3
Abx
15-75
sepsis survivors
Days 0 2/3 10/15
Microbial burden
Survival
L. pneumophila or A. fumigatus
B Sepsis
Survival (%)
naive
CLP
Days after CLP
C Second infection
naive
CLP15d
CLP30d
CLP60d
CLP75d
Days after L. pneumophila infection
D Second infection
L. pneumophila (Log CFU per lung)
naive CLP
E
naive
CLP
Days after A. fumigatus infection
F
A. fumigatus (Log CFU per lung)
naive CLP
G Sepsis
Adenosine quantification
Days 0 1 3 7 15 45 75
Abx
CLP
naive mice
H Plasma adenosine
Day 0
Day 1
Day 3
Day 7
Day 15
Day 45
Relative intensity (%)
Adenosine
Theophylline
Time (min)
I
Plasma adenosine (μM)
Days after CLP
J
Sepsis
Second infection
naive mice
CLP
Abx
A2aRi (daily)
sepsis survivors
A. fumigatus or L. pneumophila
K Second infection
naive+vehicle/naive+A2aRi
CLP+vehicle
CLP+A2aRi
Days after A. fumigatus infection
Days after L. pneumophila infection
L Second infection
vehicle
A2aRi
A. fumigatus (Log CFU per lung)
L. pneumophila (Log CFU per lung)
L. pneumophila (Log CFU per spleen)
naive CLP
M
WT
Adora2a-/-
L. pneumophila (Log CFU per lung)
L. pneumophila (Log CFU per spleen)
naive CLP

1

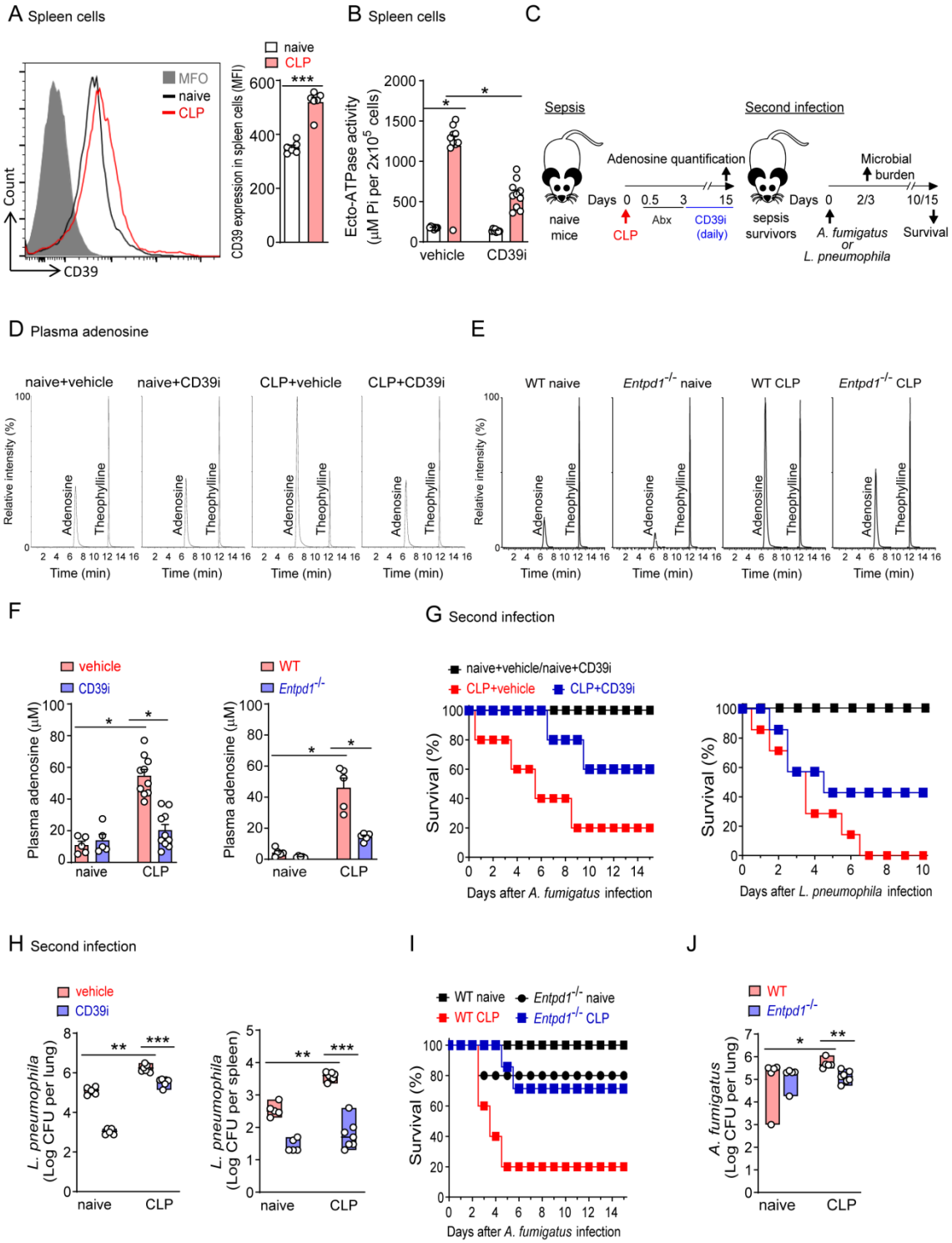
A Spleen cells
MFO
naive
CLP
Count
CD39
naive
CLP
CD39 expression in spleen cells (MFI)
B Spleen cells
Ecto-ATPase activity (μM Pi per 2x10^5 cells)
vehicle
CD39i
C
Sepsis
Second infection
Adenosine quantification
Microbial burden
naive mice
Days 0 0.5 3 15
CLP
Abx
CD39i (daily)
sepsis survivors
Days 0 2/3 10/15
A. fumigatus or L. pneumophila
Survival
D Plasma adenosine
naive+vehicle
naive+CD39i
CLP+vehicle
CLP+CD39i
Relative intensity (%)
Adenosine
Theophylline
Time (min)
E
WT naive
Entpd1-/- naive
WT CLP
Entpd1-/- CLP
F
vehicle
CD39i
Plasma adenosine (μM)
naive
CLP
WT
Entpd1-/-
G Second infection
naive+vehicle/naive+CD39i
CLP+vehicle
CLP+CD39i
Survival (%)
Days after A. fumigatus infection
Days after L. pneumophila infection
H Second infection
vehicle
CD39i
L. pneumophila (Log CFU per lung)
L. pneumophila (Log CFU per spleen)
I
WT naive
Entpd1-/- naive
WT CLP
Entpd1-/- CLP
Survival (%)
Days after A. fumigatus infection
J
WT
Entpd1-/-
A. fumigatus (Log CFU per lung)

1

Figure 3

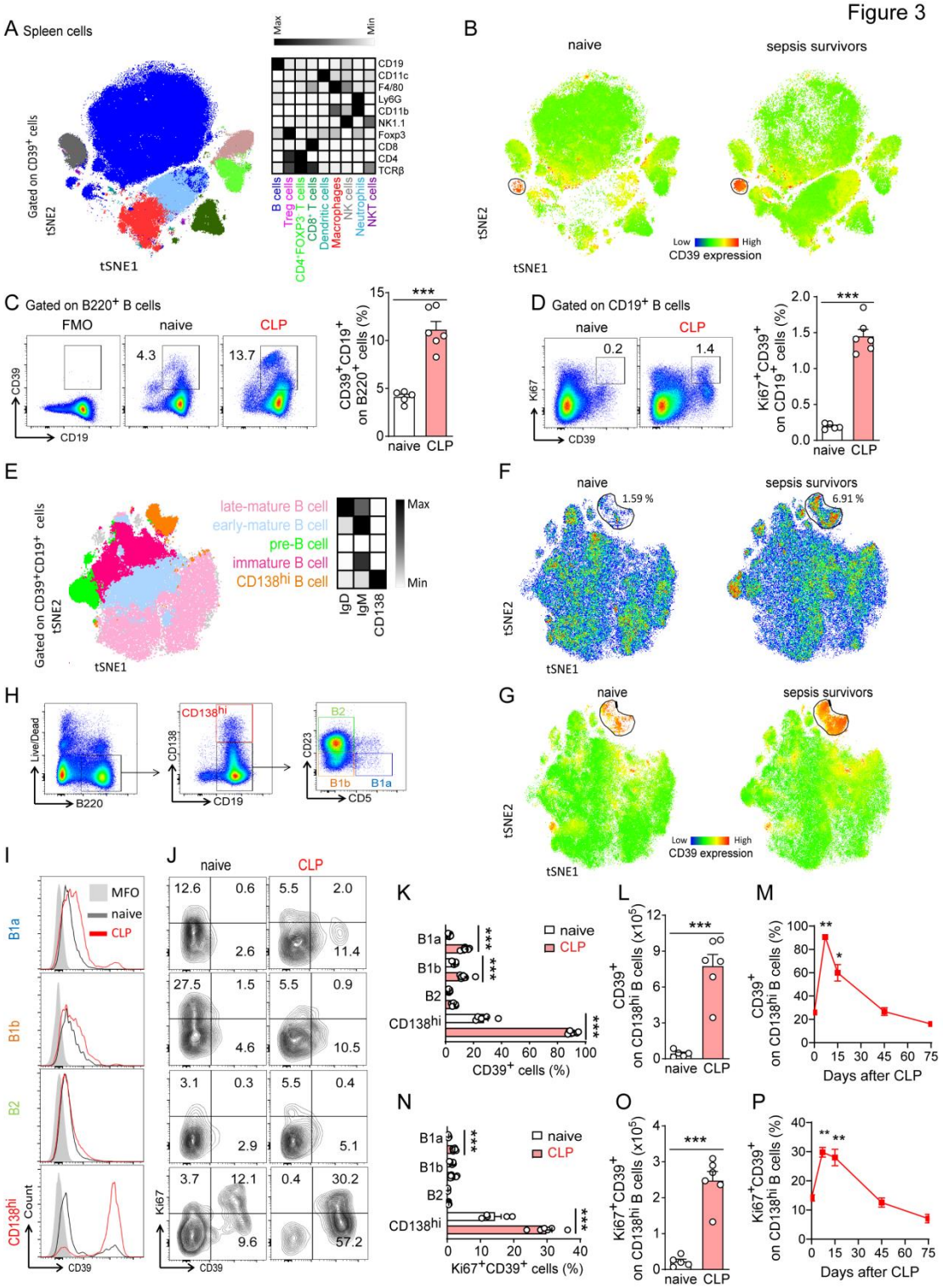
A Spleen cells
Max
Min
CD19
CD11c
F4/80
Ly6G
CD11b
NK1.1
Foxp3
CD8
CD4
TCRβ
B cells
Treg cells
CD4+FOXP3+ T cells
CD8+ T cells
Dendritic cells
Macrophages
NK cells
Neutrophils
NKT cells
Gated on CD39+ cells
tSNE2
tSNE1
B
naive
sepsis survivors
Low
High
CD39 expression
C Gated on B220+ B cells
FMO
naive
CLP
4.3
13.7
CD39
CD19
CD39+CD19+ on B220+ cells (%)
***
naive
CLP
D Gated on CD19+ B cells
0.2
1.4
Ki67
CD39
Ki67+CD39+ on CD19+ cells (%)
E
late-mature B cell
early-mature B cell
pre-B cell
immature B cell
CD138hi B cell
Max
Min
IgD
IgM
CD138
Gated on CD39+CD19+ cells
F
1.59 %
6.91 %
H
Live/Dead
B220
CD138hi
CD19
B2
B1b
B1a
CD23
CD5
G
I
MFO
naive
CLP
B1a
B1b
B2
CD138hi
Count
CD39
J
12.6
0.6
5.5
2.0
2.6
11.4
27.5
1.5
5.5
0.9
4.6
10.5
3.1
0.3
5.5
0.4
2.9
5.1
3.7
12.1
0.4
30.2
9.6
57.2
Ki67
K
CD39+ cells (%)
L
CD39+ on CD138hi B cells (x10^5)
M
CD39+ on CD138hi B cells (%)
Days after CLP
N
Ki67+CD39+ cells (%)
O
Ki67+CD39+ on CD138hi B cells (x10^5)
P
Ki67+CD39+ on CD138hi B cells (%)

1

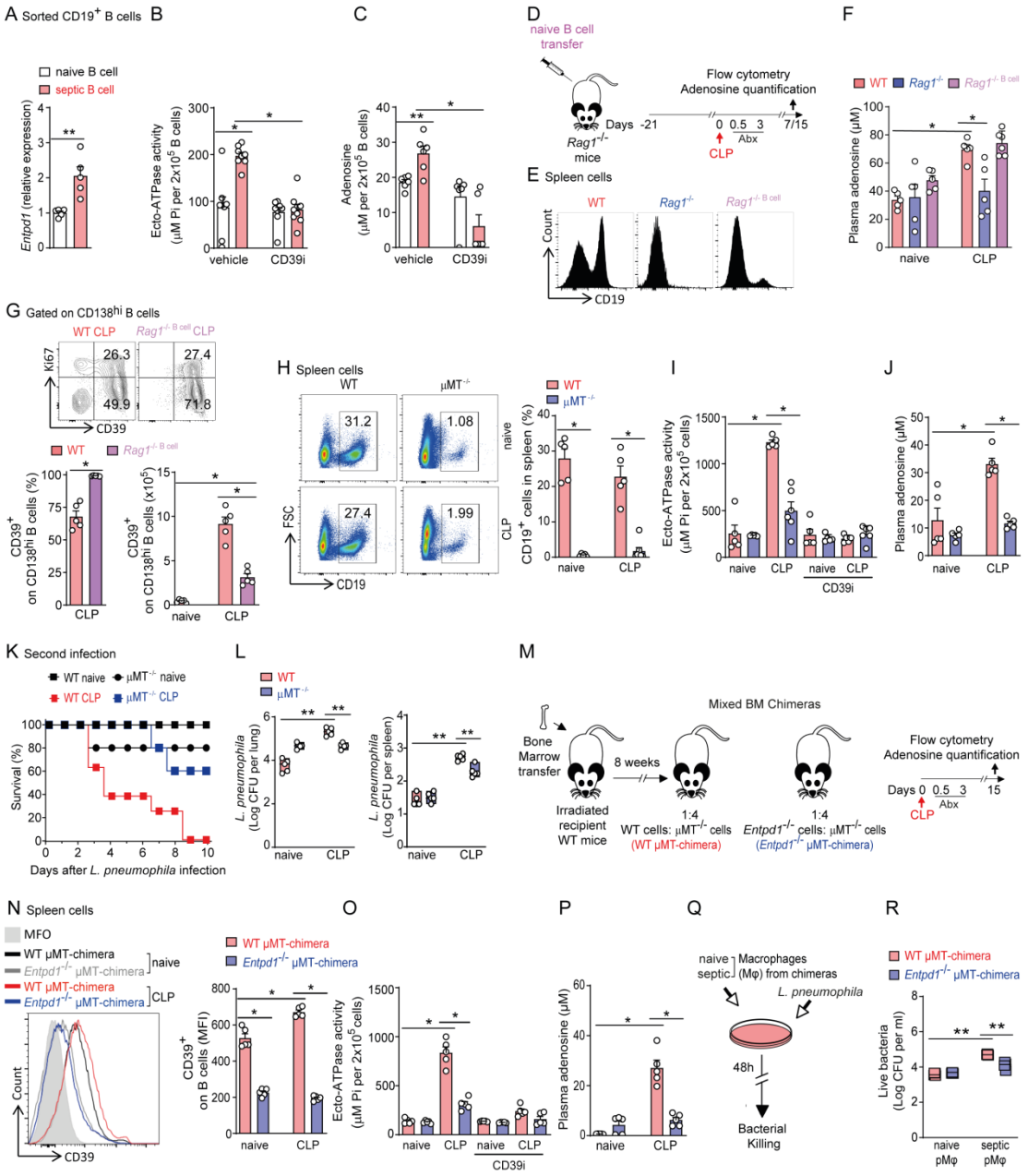
A Sorted CD19+ B cells
naive B cell
septic B cell
Entpd1 (relative expression)
B
Ecto-ATPase activity (μM Pi per 2x10^5 B cells)
vehicle
CD39i
C
Adenosine (μM per 2x10^5 B cells)
D
naive B cell transfer
Rag1-/- mice
Days -21
0 0.5 3 7/15
Abx
CLP
Flow cytometry
Adenosine quantification
E Spleen cells
WT
Rag1-/-
Rag1-/- B cell
Count
CD19
F
Plasma adenosine (μM)
naive
CLP
G Gated on CD138hi B cells
WT CLP
Rag1-/- B cell CLP
Ki67
CD39
26.3
27.4
49.9
71.8
CD39+ on CD138hi B cells (%)
CD39+ on CD138hi B cells (x10^5)
H Spleen cells
WT
μMT-/-
31.2
1.08
27.4
1.99
FSC
CD19
naive
CLP
I
CD19+ cells in spleen (%)
Ecto-ATPase activity (μM Pi per 2x10^5 cells)
CD39i
J
Plasma adenosine (μM)
K Second infection
WT naive
μMT-/- naive
WT CLP
μMT-/- CLP
Survival (%)
Days after L. pneumophila infection
L
L. pneumophila (Log CFU per lung)
L. pneumophila (Log CFU per spleen)
M
Mixed BM Chimeras
Bone Marrow transfer
Irradiated recipient WT mice
8 weeks
1:4
WT cells: μMT-/- cells
(WT μMT-chimera)
Entpd1-/- cells: μMT-/- cells
(Entpd1-/- μMT-chimera)
Flow cytometry
Adenosine quantification
Days 0 0.5 3 15
Abx
CLP
N Spleen cells
MFO
WT μMT-chimera
Entpd1-/- μMT-chimera
naive
CLP
Count
CD39
O
CD39+ on B cells (MFI)
Ecto-ATPase activity (μM Pi per 2x10^5 cells)
CD39i
P
Plasma adenosine (μM)
Q
naive
septic
Macrophages (Mφ) from chimeras
L. pneumophila
48h
Bacterial Killing
R
Live bacteria (Log CFU per ml)
naive pMφ
septic pMφ

1

Figure 5

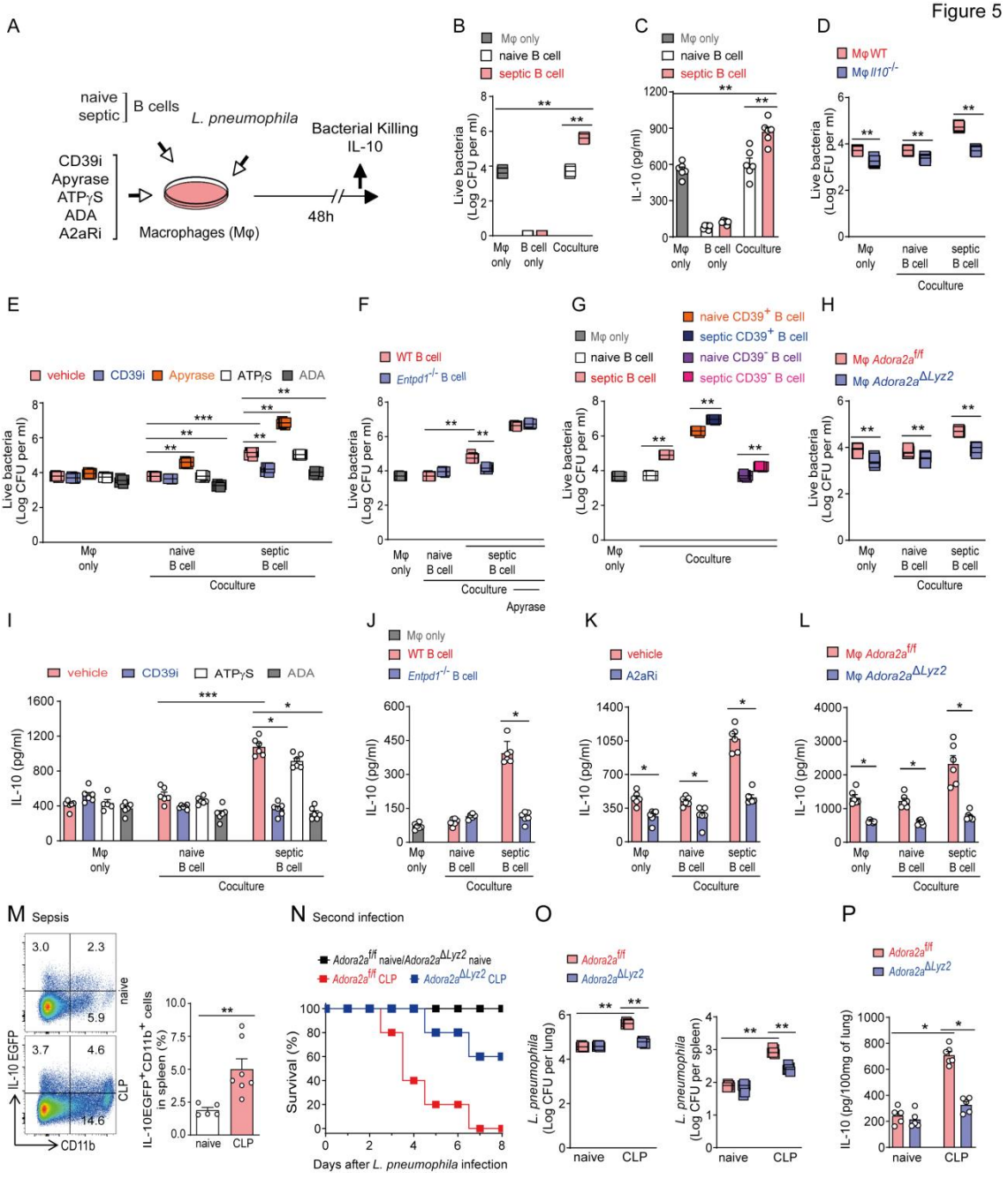
A
naive
septic
B cells
L. pneumophila
Bacterial Killing
IL-10
CD39i
Apyrase
ATPγS
ADA
A2aRi
Macrophages (Mφ)
48h
B
Mφ only
naive B cell
septic B cell
Live bacteria (Log CFU per ml)
Mφ only
B cell only
Coculture
C
IL-10 (pg/ml)
D
Mφ WT
Mφ Il10-/-
E
vehicle
CD39i
Apyrase
ATPγS
ADA
F
WT B cell
Entpd1-/- B cell
G
naive CD39+ B cell
septic CD39+ B cell
naive CD39- B cell
septic CD39- B cell
H
Mφ Adora2af/f
Mφ Adora2aΔLyz2
I
J
K
vehicle
A2aRi
L
M Sepsis
3.0
2.3
5.9
3.7
4.6
14.6
naive
CLP
IL-10 EGFP
CD11b
IL-10EGFP+CD11b+ cells in spleen (%)
N Second infection
Adora2af/f naive/Adora2aΔLyz2 naive
Adora2af/f CLP
Adora2aΔLyz2 CLP
Survival (%)
Days after L. pneumophila infection
O
Adora2af/f
Adora2aΔLyz2
L. pneumophila (Log CFU per lung)
L. pneumophila (Log CFU per spleen)
P
IL-10 (pg/100mg of lung)

1

Figure 6

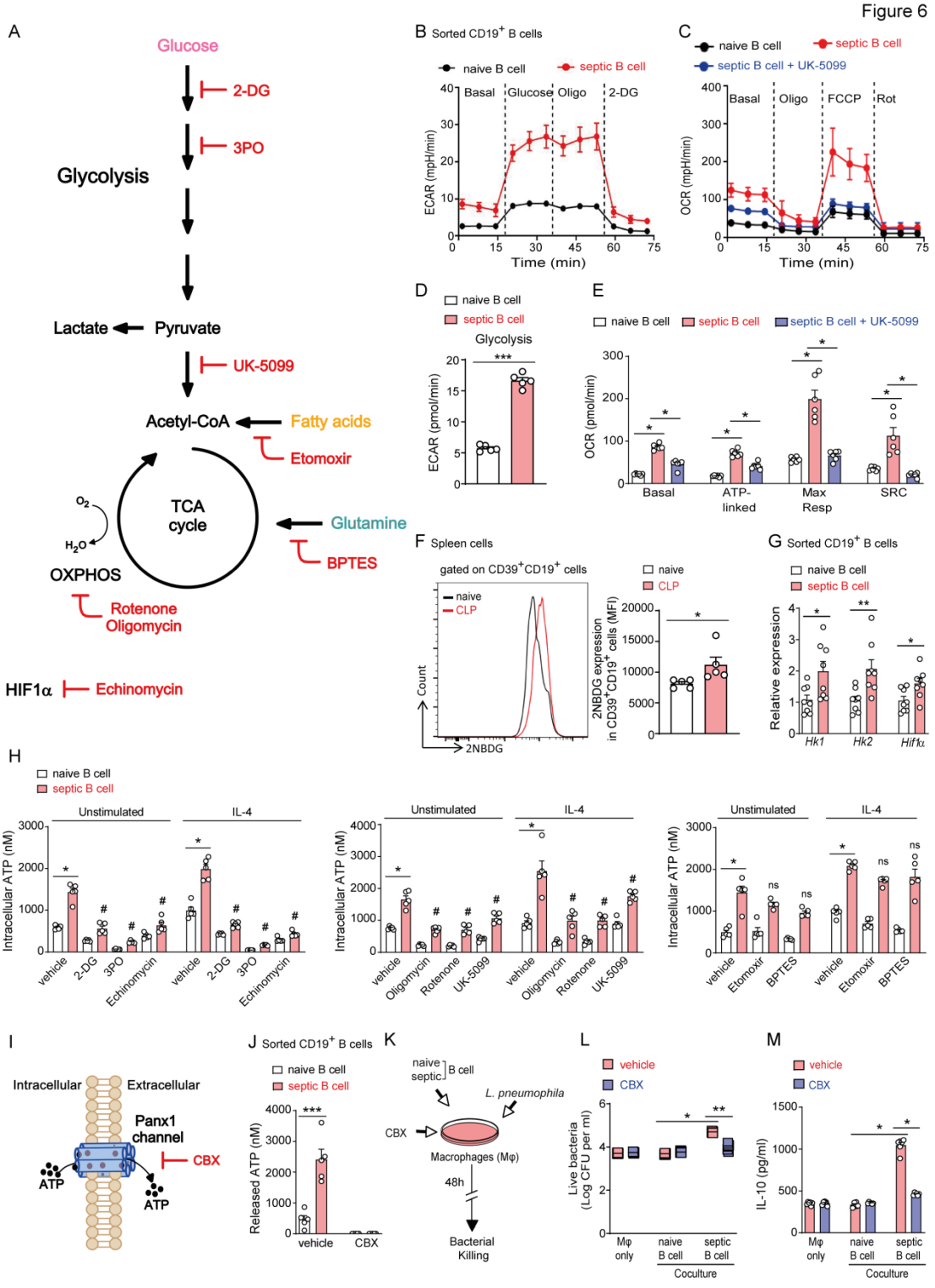
A
Glucose
2-DG
3PO
Glycolysis
Lactate
Pyruvate
UK-5099
Acetyl-CoA
Fatty acids
Etomoxir
TCA cycle
Glutamine
BPTES
OXPHOS
Rotenone
Oligomycin
HIF1α
Echinomycin
B Sorted CD19+ B cells
naive B cell
septic B cell
Basal
Glucose
Oligo
2-DG
ECAR (mpH/min)
Time (min)
C
naive B cell
septic B cell
septic B cell + UK-5099
Basal
Oligo
FCCP
Rot
OCR (mpH/min)
Time (min)
D
naive B cell
septic B cell
Glycolysis
ECAR (pmol/min)
E
naive B cell
septic B cell
septic B cell + UK-5099
OCR (pmol/min)
Basal
ATP-linked
Max Resp
SRC
F Spleen cells
gated on CD39+CD19+ cells
naive
CLP
Count
2NBDG
2NBDG expression in CD39+CD19+ cells (MFI)
G Sorted CD19+ B cells
naive B cell
septic B cell
Relative expression
Hk1
Hk2
Hif1α
H
naive B cell
septic B cell
Unstimulated
IL-4
Intracellular ATP (nM)
vehicle
2-DG
3PO
Echinomycin
Oligomycin
Rotenone
UK-5099
Etomoxir
BPTES
I
Intracellular
Extracellular
Panx1 channel
CBX
ATP
ATP
J Sorted CD19+ B cells
naive B cell
septic B cell
Released ATP (nM)
vehicle
CBX
K
naive
septic
B cell
L. pneumophila
CBX
Macrophages (Mφ)
48h
Bacterial Killing
L
vehicle
CBX
Live bacteria (Log CFU per ml)
Mφ only
naive B cell
septic B cell
Coculture
M
vehicle
CBX
IL-10 (pg/ml)
Mφ only
naive B cell
septic B cell
Coculture

FIGURE LEGENDS

FIGURE 1: Adenosine mediates sepsis-induced immunosuppression through A2aR

(A) Schematic representation of sepsis-induced immunosuppression model (B-F) (also see STAR Methods).

(B) Survival curves after CLP. Naive n=10 and CLP n=30.

(C) Survival curves of naive or CLP-surviving mice after *L. pneumophila* infection. n=5-8.

(D) Bacterial load in the lungs of naive or CLP-surviving mice 2 days after *L. pneumophila* infection. n=5-7.

(E) Survival curves of naive or CLP-surviving mice after *A. fumigatus* infection. n=5.

(F) Fungal load in the lungs of naive or CLP-surviving mice 3 days after *A. fumigatus* infection. n=5-8.

(G) Schematic representation of the experimental protocol for quantification of plasma adenosine after CLP.

(H) Representative HPLC chromatograms and (I) concentrations of plasma adenosine of naive or CLP-surviving mice. n=5-20.

(J) Schematic representation of sepsis-induced immunosuppression model with A2aR antagonist [A2aRi, 8-(3-Chlorostyryl)-caffeine, 1 $mg.kg^{-1}$] treatment (K-L) (also see STAR Methods).

(K) Survival curves of CLP-surviving mice after *A. fumigatus* or *L. pneumophila* infections. n=5.

(L) Pathogen load in the lungs of CLP-survivors after *A. fumigatus* infection and in lungs and spleen after *L. pneumophila* infection. n=5-8.

(M) Bacterial load in the lungs and spleens of CLP-surviving WT and *Adora2a*$^{-/-}$ mice after *L. pneumophila* infection. n=5.

Data are representative of 2-3 independent experiments. $^{**}p < 0.01$, $^{***}p < 0.001$. Mantel-Cox log-rank test in B, C, E, K; one-way ANOVA with Dunnett posthoc tests in I; and Mann–Whitney U test in D, F, L, M.

FIGURE 2: CD39 is required for sepsis-induced immunosuppression

(A-B) Splenic cells from CLP-surviving mice were harvested 15 days after CLP.

(A) Histogram and mean fluorescence intensity (MFI) of CD39 expression in total splenic cells. n=6.

(B) Ecto-ATPase activity of splenic cells cultured ±CD39 inhibitor (CD39i, ARL 67156, 200µM). n=8-10.

(C) Diagram of sepsis-induced immunosuppression model with CD39i (2 $mg.kg^{-1}$) treatment (D, F-H) (also see STAR Methods).

(D-E) Representative HPLC chromatograms and (F) concentrations of plasma adenosine of naïve or CLP-surviving WT, *Entpd1*$^{-/-}$ or CD39i-treated mice. n=5-10.

(G) Survival curves of CLP-surviving WT, *Entpd1*$^{-/-}$ or CD39i-treated mice after *A. fumigatus* or *L. pneumophila* infection. n=5-7.

(H) Bacterial load in the lungs and spleens of naive or CLP-surviving mice after *L. pneumophila* infection. n=5-7.

(I) Survival curves of CLP-surviving WT or *Entpd1*$^{-/-}$ mice after *A. fumigatus* infection. n=5-7.

(J) Fungal load in the lungs of CLP-surviving WT or *Entpd1*$^{-/-}$ mice after *A. fumigatus* infection. n=5-7.

Data are representative of 2-3 independent experiments. *$p < 0.05$, **$p < 0.01$, ***$p < 0.001$. Two-tailed unpaired Student's t-test in A, B, F; Mantel-Cox log-rank test in G, I; and Mann–Whitney U test in H, J.

FIGURE 3: Expansion of a CD39^{+} B cell subset in sepsis-surviving mice

(A-P) Splenic cells from CLP-surviving mice were harvested 7 or 15 days after CLP.

(A) Unsupervised analysis of single live CD39^{+} cells from the flow cytometry dataset of splenic immune cells of naïve and sepsis-surviving mice 15 days after CLP, using the t-SNE algorithm as described in STAR Methods. n=10.

(B) Heatmap density plots with MFI of CD39 expressed in different cell lineages with a blue-green-yellow-red continuous color scale. Naive n=5 and CLP n=5.

(C-D) Representative flow cytometry plots and bar graph showing (C) the frequency of splenic CD39^{+}CD19^{+} on gated B220^{+} B cells or (D) Ki67^{+}CD39^{+} on CD19^{+} B cells from naïve and sepsis survivors 7 days after CLP. n=5-6.

(E-G) Unsupervised analysis of single live CD39^{+}CD19^{+} B cells from the flow cytometry dataset of immune cells in the spleen of naïve and sepsis-surviving

mice 15 days after CLP, using the t-SNE algorithm as described in STAR Methods.

(E) t-SNE maps color-coded according to manually gated clusters of distinct $CD39^+$ B cell subsets. n=10.

(F) t-SNE maps color-coded according to cell density cluster of distinct $CD39^+$ B cell subsets. Naive n=5 and CLP n=5.

(G) t-SNE maps color-coded according to the MFI of CD39 expression intensity in distinct B cell subsets. Naive n=5 and CLP n=5.

(H-P) B cell subset gating strategy. B1a ($CD138^-CD23^-CD5^+$), B1b ($CD138^-CD23^-CD5^-$), and B2 ($CD138^-CD5^-CD23^+$) and plasmablast ($CD138^{hi}$) cells among viable $B220^+CD19^+$ cells.

(I) Histogram of CD39 expression in B1a, B1b, B2, and plasmablast cells from naïve and sepsis survivors 7 days after CLP. n=5-6.

(J, K) Representative flow cytometry plots and graph bars showing the frequency of CD39 expression in B cell subsets from naive and sepsis survivors 7 days after CLP. n=5-6.

(L) The absolute number of $CD39^+CD138^{hi}$ cells. n=5-6.

(M) Frequency of $CD39^+CD138^{hi}$ cells. n=5-6.

(J, N) Representative flow cytometry plots and graph bars showing the frequency of Ki67 and CD39 expression in B cell subsets from naive and sepsis survivors 7 days after CLP. n=5-6.

(O) The absolute number of $Ki67^+CD39^+CD138^{hi}$ cells. n=5-6.

(P) Frequency of $Ki67^+CD39^+CD138^{hi}$ cells. n=5-6.

Data are representative of 2-3 independent experiments. *p < 0.05, **p < 0.01, ***p < 0.001. Two-tailed unpaired Student's t-test in C, D, K, N, L, O and one-way ANOVA with Dunnett posthoc tests in M, P.

FIGURE 4: $CD39^+$ B cells promotes immunosuppression in sepsis-surviving mice

(A-C) Splenic $CD19^+$ B cells were isolated from CLP-surviving mice 15 days after CLP.

(A) mRNA expression of *Entpd1*. n=5.

(B) Ecto-ATPase activity ±CD39i. n=8-9.

(C) Concentration of adenosine in the cell culture supernatant. n=6.

(D) A diagram of B cell transfer into *Rag1*$^{-/-}$ mice following by sepsis-induced immunosuppression model (E-G) (also see STAR Methods).

(E) Flow cytometry analysis of CD19^{+} splenic cells from WT, *Rag1*$^{-/-}$ and *Rag1*$^{-/-}$ $^{B\ cell}$ (B cell transferred) mice 15 days after CLP. n=5-7.

(F) Plasma adenosine concentrations from sepsis survivors 15 days after CLP. n=5-7.

(G) Representative flow cytometry plots and graph bars showing the frequency and the absolute number of splenic CD39^{+}CD138^{hi} B cells from sepsis survivors 7 days after CLP. n=5.

(H-L) Sepsis-surviving WT and µMT$^{-/-}$ mice were challenged with *L. pneumophila* 15 days after CLP.

(H) Representative flow cytometry plots and graph bars showing the frequency of splenic CD19^{+} B cells from WT and µMT$^{-/-}$ mice 15 days after CLP. n=5-7.

(I) Ecto-ATPase activity in splenic cells from WT and µMT$^{-/-}$ mice cultured ±CD39i. n=5-6.

(J) Plasma adenosine concentration in WT and µMT$^{-/-}$ mice 15 days after CLP. n=5.

(K) Survival curves of WT and µMT$^{-/-}$ mice after *L. pneumophila* infection. n=5-8.

(L) Bacterial loads in the lungs and spleens from WT and µMT$^{-/-}$ mice after *L. pneumophila* infection. n=5.

(M) A diagram of mixed bone marrow (BM) cells reconstitution in irradiated recipient all mice following by sepsis-induced immunosuppression model (N-P) (also see STAR Methods).

(N) Histogram and MFI of CD39 expression on CD19^{+} B cells. n=5.

(O) Ecto-ATPase activity of splenic cells cultured in ±CD39i. n=5.

(P) Plasma adenosine concentration. n=5.

(Q) A diagram of peritoneal macrophages (Mφ) from naive or sepsis-surviving chimeras exposed to *L. pneumophila in vitro* for analysis of killing assay.

(R) The number of viable bacteria recovered from Mφ lysates. n=5.

Data are representative of 2-3 independent experiments. *$p < 0.05$, **$p < 0.01$ Two-tailed unpaired Student's t-test in A-C, G-H, J, N-P; one-way ANOVA with Bonferroni posthoc tests in F, I; Mantel-Cox log-rank test in K; and Mann–Whitney U test in L, R.

FIGURE 5: Septic B cell-derived adenosine impairs macrophage bacterial

(A) Schematic representation of bacterial killing and IL-10 production analysis by Mφs co-cultured with naive or septic B cells in the presence of *L. pneumophila* determined after 48h (B-L) (also see STAR Methods). Naive peritoneal macrophages were pooled from 5 naive mice and B cells were isolated from naïve or CLP-surviving mice. n=6.

(B) The number of viable bacteria recovered from cell lysates.

(C) Concentrations of IL-10 in cell supernatant.

(D) The number of viable bacteria recovered from lysates of naive WT and *Il10*$^{-/-}$ macrophages and/or naive or septic B cells.

(E-F) The number of viable bacteria recovered from lysates of naive macrophages with naive or septic *Entpd1*$^{-/-}$ or WT B cells in the presence of CD39i, Apyrase (20 U.mL^{-1}), ATPɣS (100 µM), ADA (4 U.mL^{-1}).

(G) The number of viable bacteria recovered from lysates of naive macrophages and/or naive or septic CD39^{+} or CD39^{-} B cells.

(H) The number of viable bacteria recovered from lysates of naive, *Adora2a*$^{f/f}$ or *Adora2a*$^{\Delta Lyz2}$ macrophages and/or naive or septic B cells.

(I-K) Concentrations of IL-10 in the culture supernatants of naive, *Adora2a*$^{f/f}$ or *Adora2a*$^{\Delta Lyz2}$ macrophages with naive or septic *Entpd1*$^{-/-}$ B cells in the presence of CD39i, ATPɣS, ADA and A2aRi (100 µM).

(M) Representative flow cytometry dot plots and frequency of splenic IL-10-EGFP^{+}CD11b^{+} cells 15 days after CLP. n=5-7.

(N-P) Sepsis-surviving *Adora2a*$^{f/f}$ and *Adora2a*$^{\Delta Lyz2}$ mice were challenged with *L. pneumophila* 15 days after CLP, n=5-6.

(N) Survival curves after *L. pneumophila* infection.

(O) Bacterial loads in the lungs after *L. pneumophila* infection.

(P) IL-10 concentrations in the lungs after *L. pneumophila* infection.

Data are representative of 2-3 independent experiments. *p < 0.05, **p < 0.01, ***p < 0.001. Mann–Whitney U test in B, D-H, O; two-tailed unpaired Student's t-test in C, I-M, P; and Mantel-Cox log-rank test in N.

FIGURE 6: Sepsis induces alterations in B cell metabolic reprogramming

(A) Schematic representation detailing pharmacological inhibitors for the metabolic pathways required for ATP generation.
(B-E) $CD19^+$ B cells were isolated from naive or sepsis-surviving mice and cultured with IL-4 for 6 h ±UK-5099 (20 μM).
(B) Kinetic profile of extracellular acidification rate (ECAR) measured by Seahorse under basal condition and in response to glucose, oligomycin, and 2-DG at the indicated time points. n=5.
(C) Kinetic profile of oxygen consumption rate (OCR) measured by Seahorse, under basal condition, and in response to oligomycin, FCCP, and rotenone at the indicated time points. n=6.
(D) Maximal glycolysis calculated from ECAR profile. n=5.
(E) Basal respiration, ATP-linked, maximal respiration, and spare respiratory capacity (SRC) calculated from OCR profile. n=6.
(F) Flow cytometry histogram and graph bar showing MFI for 2NBDG in $CD39^+CD19^+$ B cells. n=5.
(G) mRNA expression of *Hk1*, *Hk2*, *Hif1α* in $CD19^+$ B cells determined by qPCR. n=8.
(H) Intracellular ATP quantified in lysates of $CD19^+$ B cell stimulated with IL-4 in the presence of 2-DG, 3PO, echinomycin, oligomycin, rotenone, UK-5099, etomoxir or BPTES. n=5.
(I) Illustration showing the simplified representation of the ATP release via the pannexin-1 channel and inhibition with carbenoxolone (CBX, 100 μM).
(J) Extracellular ATP quantified in the cell culture supernatant of $CD19^+$ B cells stimulated with IL-4 ±CBX. n=5.
(K) Schematic representation of bacterial killing and IL-10 production analysis by Mφs co-cultured with naive or septic B cells in the presence of *L. pneumophila* ± CBX determined after 48h (B-L) (also see STAR Methods). Naive peritoneal macrophages were pooled from 5 naive mice and B cells were isolated from naïve or CLP-surviving mice. n=6.
(L) The number of viable bacteria recovered from cell lysates.
(M) IL-10 concentrations in cell culture supernatants.
Data are representative of one 2-3 independent experiments. ns, not significant. *$p < 0.05$, **$p < 0.01$, ***$p < 0.001$ between indicated groups and #$p<0.05$:

compared to respective vehicle group. ns, not significant. One-way ANOVA with Bonferroni posthoc tests in B, C, E; two-tailed unpaired Student's t-test in D, F-H, J, M; and Mann–Whitney U test in L.

FIGURE 7: Characterization of $CD39^+$ B cells in septic patients

(A) Representative flow cytometry plots and graph bar showing the frequency of $Ki67^+CD39^+$ in $CD19^+$ B cells from blood of septic patients (n=18) and healthy controls (n=16).

(B) Gating strategy for the identification of human blood B cell subsets. Naive B cells ($CD38^-CD27^-$), memory B cells ($CD38^-CD27^+$), and plasmablasts ($CD38^+CD27^+$) gated in viable $CD19^+$ B cells from blood of septic patients (n=21) and healthy controls (n=21).

(C) Representative flow cytometry plots of CD39 expression in B cell subsets from septic patients (n=21) and healthy controls (n=21).

(D) Frequency of CD39 high (hi), intermediate (int), and negative (neg) expression in plasmablast cells from septic patients (n=21) and healthy controls (n=21).

(E) Ecto-ATPase activity of $CD19^+$ B cells sorted from septic patients (n=20) and healthy controls (n=21) cultured ±CD39i.

(F) Plasma adenosine concentrations in septic patients (n=21) and healthy controls (n=36).

(G) Plasma adenosine concentrations in patients with sepsis (n=8) or septic shock (n=13) and healthy controls (n=36).

(H) Correlation between Ecto-ATPase activity of $CD19^+$ B cells and plasma adenosine concentration for each septic patient (n=20).

(I, J) $CD14^+$ monocytes (Mφ) isolated from blood of a healthy donor were co-cultured with septic or healthy B cells in the presence of *L. pneumophila* expressing luciferase at a MOI of 0.01 and A2aRi, apyrase or vehicle.

(I) Bacterial load determined by measuring the luminescence (RLU) on day 3 after culture.

(J) IL-10 concentration in the cell culture supernatants.

(K-L) Single-cell RNA-sequencing data of blood cells from individuals with sepsis (Reyes et al., 2020).

(K) UMAP reduction plot of B cells from individuals with no sepsis (left) or patients with sepsis (right). The cells in black represent the plasmablast cells according to markers utilized by the original article.
(L) Relative frequency of plasmablast in patients with no sepsis (black) and with sepsis (orange).
*, $p < 0.05$: compared to vehicle healthy B cell group. #, $p < 0.05$: compared to vehicle group of each individual. Two-tailed unpaired Student's t-test in A, F; one-way ANOVA with Bonferroni posthoc tests in D, E, G, J; *p*-value and correlation coefficient (r) were obtained using the nonparametric Spearman rank correlation test in H; and Mann–Whitney U test in I.

STAR METHODS

RESOURCE AVAILABILITY

Lead contact

Further information and requests for reagents may be obtained from the Lead Contact, José Carlos Alves-Filho (jcafilho@usp.br).

Materials availability

This study did not generate new or unique reagents.

Data and code availability

This paper analyzes existing, publicly available data from (Reyes et al., 2020) at Broad Institute Single Cell Portal (https://singlecell.broadinstitute.org/single_cell): SCP548 (subject PBMCs). These accession numbers for the datasets are listed in the key resources table. All software and algorithms used in this study are publicly available and listed in the Key Resource table. All original code has been deposited and is publicly available at Zenodo https://doi.org/10.5281/zenodo.4922037. DOIs are listed in the key resources table.

EXPERIMENTAL MODEL AND SUBJECT DETAILS

Animals

C57BL/6 wild-type and BALB/c wild-type mice were purchased from Charles River. µMT$^{-/-}$ (002288), *Adora2a*$^{-/-}$ (010685), Foxp3-DTR-EGFP (016958), *Il10*$^{-/-}$ (002251), IL-10$^{+/EGFP}$ (014530), *Lyz2*^{Cre} (004781) and *Rag1*$^{-/-}$ (002216) mice were purchased from the Jackson Laboratory. *Entpd1*$^{-/-}$ mice were generated as previously described (Enjyoji et al., 1999) and kindly provided by Dr. Gilles Kauffenstein. *Adora2a*^{flox} mice were generated as previously described (Cekic et al., 2013) and kindly provided by Dr. Joel Linden. Myeloid cell-(*Adora2a*$^{\Delta Lyz2}$) specific–*Adora2a*-deficient mice were generated by crossing the *Adora2a*$^{flox/flox}$ mice with *Lyz2*^{Cre} mice. µMT$^{-/-}$, *Adora2a*^{flox}, *Entpd1*$^{-/-}$, Foxp3-DTR-EGFP, *Il10*$^{-/-}$, IL-10$^{+/EGFP}$, *Lyz2*^{Cre}, and *Rag1*$^{-/-}$ mice used in this study were on a C57BL/6 background. *Adora2a*$^{-/-}$ mice used in this study were on a BALB/c J background. All mice were bred and maintained under specific pathogen-free conditions at the

Animal Facility of the Ribeirão Preto Medical School, University of São Paulo. All experiments were carried out with 7-9-week-old male mice according to the guidelines of the Animal Welfare Committee of the Ribeirão Preto Medical School, University of São Paulo (protocol number: 070/2012 and 251/2019).

Patients

Adult patients admitted to the Emergency Department of the School of Medicine of Ribeirão Preto with sepsis or septic shock between October 2020 and December 2020 were enrolled in the study (Table S1). Besides, age- and sex-matched healthy control volunteers were also included in the study. All patients enrolled fulfilled the criteria defined by the Third International Consensus Definitions for Sepsis and Septic Shock (Sepsis-3) (Singer et al., 2016). The exclusion criteria included active hematological malignancy or cancer and transplantation. Informed written consent from all participants was obtained. The study was approved by the Human Subjects Institutional Committee of the Ribeirão Preto Medical School, Brazil (Licence number: 30459114.6.0000.5440).

Caecal ligation and puncture (CLP)-induced polymicrobial sepsis model

CLP-induced polymicrobial sepsis model (Rittirsch et al., 2009): Mice were anesthetized by inhalation administration of isoflurane (1-3 %), and two punctures were made in the caecum with an 18- or 23-gauge needle to induce lethal or moderate CLP-induced sepsis, respectively. Sham mice were submitted to the same procedures without caecal puncture. All mice were given analgesic (12.5 $mg.kg^{-1}$, tramadol, Agener União, subcutaneous) beginning 30 min before CLP and then every 12 h up to day 3. To increase the survival rates after lethal sepsis (Nascimento et al., 2010), C57BL/6 background mice received an i.p. injection of ertapenem sodium (30 $mg.kg^{-1}$, Merck) beginning six h after CLP and continuing every 12 h for the first three days. In experiments performed on BALB/c background, mice received antibiotics up to day 4. In some experiments, septic mice were treated with A2aR antagonist [8-(3-Chlorostyryl)-caffeine, 1 $mg.kg^{-1}$ in DMSO 5 % in PBS], or CD39 inhibitor (ARL 67156 trisodium salt, 2 $mg.kg^{-1}$ in PBS). Mice were injected intraperitoneally with an A2aR antagonist or CD39 inhibitor (200 µL) beginning on day three and continuing for 12 consecutive days (once a day). Survival was observed for up to 15 days.

Microbial infection

Legionella pneumophila infection (Zamboni et al., 2006): *L. pneumophila* (F2111) was kindly provided by Dr. Paul Edelstein (Edelstein et al., 2003). *L. pneumophila* was grown on charcoal yeast extract agar (10 $g.L^{-1}$ 4-morpholinepropanesulfonic acid [MOPS], 10 $g.L^{-1}$ Yeast extract, pH6.9, 15 $g.L^{-1}$ bacteriological agar, 2 $g.L^{-1}$ activated charcoal, supplemented with 0.4 $g.L^{-1}$ L-cysteine and 0.135 $g.L^{-1}$ Fe(NO3)3) at 35–37 °C, for 4 days from frozen stocks. Single colonies were streaked on fresh plates and allowed to grow for another 2 days. For *in vivo* infections (Nascimento et al., 2010), mice were intranasally given a single dose of *L. pneumophila* (7 x 10^7 bacteria in 40 µL).

Aspergillus fumigatus infection: *A. fumigatus* (strain CBS 144.89) was kindly provided by Dr. Jean-Paul Latge (Beauvais et al., 1997). Conidia were grown on 15 $g.L^{-1}$ cristomalt-D diastase malt powder and 15 $g.dL^{-1}$ bacteriological agar slants at 35–37 °C for 24 h and allowed to grow at room temperature for another six days. For *in vivo* infections, mice were intratracheally given a single dose of *A. fumigatus* (5 x 10^7 bacteria in 50 µL).

Survival was observed for up to 10 days.

Cell purifications

Primary mouse $CD19^+$ B cells were purified from the spleen of mice using a FACSAriaII sorter (BD Biosciences). Cell purity was confirmed to be ≥ 95 %. Peritoneal cells of mice were enriched for macrophages by adherence to plastic Petri dishes for 16 h. Peripheral blood mononuclear cells (PBMC) were isolated from human peripheral blood using the ficoll-Paque Plus gradient (GE Healthcare). Primary human $CD19^+$ B cells were isolated by positive selection from PBMCs using CD19 MACS beads Multisort (Miltenyi Biotec) according to the manufacturer's recommendations. Cell purity was confirmed to be ≥ 95 %. Primary human $CD14^+$ monocytes were purified by positive selection from PBMCs using CD14 MACS beads Multisort (Miltenyi Biotec) according to the manufacturer's recommendations. Cell purity was confirmed to be ≥ 95 %.

B Cell Adoptive transfer

Two protocols were used. First, for reconstitution of *Rag1*$^{-/-}$ mice (Guzik et al., 2007): B cells or vehicle (PBS) were injected i.v. into *Rag1*$^{-/-}$ mice (2 x 10^7 cells/mouse). The recipient mice were then submitted to CLP 3 weeks after adoptive transfer. Second, to evaluate the role of septic B cells in the control of bacterial replication (Nascimento et al., 2017): B cells or vehicle (PBS) were injected i.v. into naïve WT mice (5 x 10^6 cells/mouse). The naïve recipient mice were then infected i.n. with *L. pneumophila* on day 7 after adoptive transfer.

Generation of B cell chimeric mice

For the generation of chimeric mice (Tsui et al., 2018), *Entpd1*$^{-/-}$, µMT$^{-/-}$, and C57BL/6 bone marrow cells were obtained by flushing the femur and tibia. C57BL/6 mice (12-weeks-old) were irradiated using a Cesium 137 source irradiator (Mark I model 25) at 7 Gy. On the day after irradiation, the mice were divided into the following groups: (1) C57BL/6 mice repopulated with a mix of C57BL/6 BM cells and µMT$^{-/-}$ BM cells in proportion 1:4 (i.v.; 5 x 10^6/mouse), called WT µMT-chimera; (2) C57BL/6 mice repopulated with a mix of *Entpd1*$^{-/-}$ BM cells and µMT$^{-/-}$ BM cells, called *Entpd1*$^{-/-}$ µMT-chimera. After bone marrow transplantation, the mice were treated with the antibiotic Ciprofloxacin hydrochloride diluted in drinking water (10 mg.mL^{-1}, EMS) for 15 days. After 2 months (period required for bone marrow engraftment), mice were submitted to CLP and were killed on day 15 after CLP.

Bacterial replication on macrophage in co-culture with B cells

For mouse samples: peritoneal macrophages from naïve mice were added to 48-well plates at a density of 5 x 10^5 cells per well. Cells were infected by 0.1 MOI *L. pneumophila* bacteria in the presence of B cells from the spleen of sepsis-surviving or naive mice or medium alone. In some experiments, we added CD39i (ARL 67156 200 µM, Tocris), Apyrase (20 U.mL^{-1}, Sigma), ATPɣS (100 µM, Tocris), ADA (4 U.mL^{-1}, Sigma), NECA (10 µM, Tocris), A2aR antagonist (8-(3-Chlorostyryl) caffeine, A2aRi, 100 µM, Sigma), A2B antagonist (selective inverse agonist, A2bRi, MRS 1706, 100 µM, Tocris), CBX (carbenoxolone disodium salt, 100 µM, Sigma) in the cultures. There were no antibiotics in the cell culture medium used for bacterial infection. On the second day, the supernatants were collected; cells were lysed with sterile H_20 and plated for counted of counting of

colony-forming units (CFU) after 4 days of incubation at 37 °C (Nascimento et al., 2010). The results are expressed as log CFU per mL.

For human samples: monocytes from the periphery blood of healthy volunteers were co-cultured with septic or healthy B cell in 96-well white plates at a density of 1 x 10^5 for each type of cells per well (triplicate). *L. pneumophila* strains (JR32) stably expressing the *Photorhabdus luminescens luxCDABE operon* was kindly provided by Dr. Dario Zamboni (Gonçalves et al., 2019). *L. pneumophila* was grown on charcoal yeast extract agar (10 $g.L^{-1}$ 4- orpholinepropanesulfonic acid [MOPS], 10 $g.L^{-1}$ Yeast extract, pH6.9, 15 $g.L^{-1}$ bacteriological agar, 2 $g.L^{-1}$ activated charcoal, supplemented with 0.4 $g.L^{-1}$ L-cysteine and 0.135 $g.L^{-1}$ Fe(NO3)3) at 35–37 °C, for 4 days from frozen stocks. Single colonies were streaked on fresh plates and allowed to grow for another 2 days. Cells were infected by *L. pneumophila* bacteria expressing luciferase at an MOI of 0.01 in the presence of A2aRi (8-(3-Chlorostyryl) caffeine, 100 µM, Sigma) or Apyrase (20 $U.mL^{-1}$, Sigma). There were no antibiotics in the cell culture medium used for bacterial infection. On the third day, luminescence emission was measured at 470 nm with a Spectra-L plate reader (Molecular Devices, California, USA), and the supernatants were collected. The results are expressed as live bacteria (RLU).

METHODS DETAILS

Adenosine quantification

Blood collection and sample preparation. For adenosine quantification in plasma (Veras et al., 2015), blood was collected in tubes containing 10 µM of pentostatin (adenosine deaminase inhibitor, Tocris) and heparin (for mouse) or K_3EDTA (for human). Blood samples were centrifuged at 10,000 × *g* for 10 min at 4 °C, and plasma was stored at −80 °C until the analyses. For adenosine quantification in the plasma, theophylline (internal standard) and 1 mL of acetonitrile were added in 200 µL of plasma. The tube was vortexed for 2 min, centrifuged at 10,000 × *g* for 10 min at 4 °C, and the supernatants were evaporated by a vacuum concentrator system (CentriVap, Labcongo Corporation). The dry residue was resuspended in 100 µL of mobile phase (water with 0.1 % formic acid). A similar protocol was used to adenosine the curve. The different concentrations of

adenosine (Sigma) were added to the plasma (collected without adenosine deaminase inhibitor) together with theophylline (internal standard). Samples (100 µL) were analyzed by LC-MS/MS using a previously described method (Veras et al., 2015).

For adenosine detection in the supernatant, B cells from sepsis-surviving mice were stimulated with ATP (100 µM, Sigma) by 15 min. At the end of the cultures, the supernatants were precipitated with 66 % acetonitrile (J. T. Baker) to denature protein stabilize adenosine and diluted 33 % in water for adenosine analysis. Different concentrations of adenosine (Sigma) were prepared in methanol to construct a standard curve.

LC-MS/MS equipment and conditions. For adenosine quantification in plasma, the analyses were carried out by LC-MS/MS (liquid chromatography-mass spectrometry). Chromatographic analyzes were performed using high-performance liquid chromatography equipment (Shimadzu, Kyoto, Japan), consisted of an LC-10ADVP binary solvent delivery pumps, SLC-10AVP system controller, SIL-20A Prominence autosampler, and CTO-10ASVP column oven set at 25 °C. The separations were performed using a 100 × 3.9 mm XTerra MS C18 column with a particle size of 3.5 µm (Waters, Milford, MA, USA) and a 20 × 3.9 mm XTerra MS C18 guard column with a particle size of 5 µm (Waters, Milford, MA, USA). The mobile phase was composed of (X) water with 0.1 % formic acid and (Y) acetonitrile. The binary gradient elution (X: Y proportion, v/v), at a flow rate of 0.3 mL.min^{-1}, was composed by 96:4 from 0 to 5 min; switching to 50:50 from 5 to 7 min; maintained by 11 min; switching back to the initial condition from 11 to 13 min, and maintaining on this proportion till 16 min. This system was coupled to a mass spectrometer composed of mass analyzers of the triple-quadrupole type (Quattro LC, Micromass, Manchester, UK) with an electrospray interface, operating in positive mode (ESI +). The temperatures of the source block were set at 100 °C, and desolvation gas was set at 350 °C. Argon was used as collision gas, and nitrogen was used as both desolvation (nearly 360 L.h^{-1}) and nebulizer (nearly 40 L.h^{-1}) gas. During the analyses, the voltages employed in the ESI source were 3kV for the capillary, 3V for the extractor, and 20V for the cone. The ions detection was carried out in the multiple reaction monitoring (MRM) mode, employing collision energy of 15 eV, monitoring

the transitions of the m/z 268 precursor ion to the m/z 136 production for adenosine (268 > 136) and 181 > 124 for theophylline (internal standard). The analytical data were calculated using the MassLynx software (Micromass, Manchester, UK).

For adenosine detection in the supernatant, samples or standards (100 µL) were injected in a Xevo TQ-S system Waters Acquity UPLC HSS with column C18 Acuity UPLC HSS with 1,0x150 mm (liquid chromatography separation). The temperature of the column oven was set at 40 °C. The solvent system consisted of 0.1 % acetic acid in water and 0.1 % acetic acid in methanol. The flow rate was set to 500 µL/min, and an injection volume of 5 µL was used with a total run time of 4.5 min. The ion positive fragment m/z 268 and 136 were observed. The analytical data were processed by MassLynx software (Micromass, Manchester, UK).

Microbial counts

On day 2 (for *L. pneumophila)* or 3 (for *A. fumigatus*) after infection, lungs and/or spleen were collected and homogenized for 30 s with a PowerGen 125 homogenizer (Fisher Scientific) in sterile H_2O (Nascimento et al., 2010). Dilutions of lung and spleen lysates were plated on charcoal yeast extract agar for the determination of CFU per organ.

Flow cytometry

Flow cytometric staining was performed as previously described (Nascimento et al., 2017). For mouse staining, Foxp3 EGFP, µMT$^{-/-}$, WT cells were stained with Live/Dead viability dye (Thermo Fisher Scientific) and specific antibodies to CD39 (24DMS1 and Duha59, Thermo Fisher Scientific and BioLegend), CD19 (1D3, Thermo Fisher Scientific or BD Biosciences; 6D5, BioLegend), CD11b (M1/70, Thermo Fisher Scientific), CD11c (N418, BioLegend), CD4 (RM4-5, BioLegend), B220 (CD45R; RA3-6B2, BioLegend or BD Bioscience), CD8 (YTS156.7.7, BioLegend), TCRβ (H57-597, Thermo Fisher Scientific), NK1.1 (PK136, BioLegend), Ly6G (1A8, BD Biosciences), CD223 (LAG-3, C9B7W, Biolegend), IgM (RMM-1, BioLegend), IgD (11-26c.2a, BD Biosciences), CD138 (281-2, BioLegend), CD3 (17A2, Thermo Fisher Scientific), CD5 (53-7.3, BD Biosciences), CD23 (B3B4, Thermo Fisher Scientific), CD21/CD35 (CR2/CR1;

7E9, BioLegend), Ki67 (B56, BD Biosciences), and CD45 (30-F11, BioLegend) for 30 min. For human cells stanning, PBMC were stained with Live/Dead viability dye (Thermo Fisher Scientific) and specific antibodies to CD39 (TU66, BD Biosciences), CD19 (HIB19, BD Biosciences), CD38 (HIT2, BD Biosciences), CD27 (M-T271, BD Biosciences), Ki67 (20Raj1, Thermo Fisher Scientific) for 30 min. For 2-NBDG uptake detection (Thermo Fisher Scientific), the reaction was stopped by removing the incubation medium and washing the cells twice with PBS. Cells were subsequently stained with Live/Dead viability dye (Thermo Fisher Scientific)and specific antibodies to CD39 and CD19 for 10 min, and flow cytometry analysis was performed within 30 min. For IL-10 detection, IL-10 EGFP cells were incubated with phorbol-12-myristate-13-acetate (50 $ng.mL^{-1}$, Sigma-Aldrich), ionomycin (500 $ng.mL^{-1}$, Sigma-Aldrich), and GolgiStop (BD Biosciences) for 4 h prior to antibody staining. Fresh cells were collected on Canto, Verse, and Fortessa flow cytometers (BD Biosciences) and analyzed using FlowJo (TreeStar) software. Cells were sorted using a FACS Aria II.

High-dimensional flow cytometric analyses

High-dimensional flow cytometric analysis of the $CD39^+$ expression on the cell populations from the spleen of naïve and sepsis-surviving mice were performed in immune cells based on the following gate strategies, on the live $CD45^+$ cells: neutrophils ($Ly6G^+CD11b^+$), Mφ ($F4/80^+CD11b^+$), DCs ($CD11c^+CD11b^+$), $CD4^+Foxp3^-$ T cells ($Foxp3^-CD4^+TCR\beta^+$), $CD8^+$ T cells ($CD8^+TCR\beta^+$), $CD4^+Foxp3^+$ Treg cells ($Foxp3^+CD4^+TCR\beta^+$), B cells ($CD19^+$ $B220^{var}$), NK cells ($NK1.1^+$) and NKT cells ($NK1.1^+TCR\beta^+$). The t-SNE algorithm was performed for unsupervised analysis of the entire flow cytometry dataset (10 samples per experiment) generated from naïve and sepsis-surviving mice. The t-SNE algorithm was run on the DownSample of live $CD45^+$ $CD39^+$ populations [100,000 cells, randomly selected from naïve (n=5) and sepsis survivors (n= 5), 50,000 cells each group)]. Flow cytometry-based immune cell populations were overlaid as a color dimension. For the B cells subpopulation analysis, cells were gated on the live $CD45^+$ as follows: total B cells ($CD19^+$ $CD3^{neg}$), CD39 subset ($CD39^+$), IgD+ subset (IgD^+ IgM^{neg}), IgD+ IgM+ subset (IgD^+ IgM^+), IgDneg IgMneg subset (IgD^{neg} IgM^{neg}), and CD138+ subset ($CD138^+$). t-SNE was run on the DownSample of 150,000 live $CD39^+CD19^+$ cells randomly sampled from the

spleen of naïve and sepsis-surviving mice (n=5 per group and 75,000 cells from each group). Gating strategies for flow cytometry analysis are shown in Figures S3A and S3E.

Ecto-ATPase activity

The ecto-ATPase activity was determined by the malachite green assay, with some modifications as described (Peres et al., 2015). Splenic or B cells (2 x10^5 cells/well for mouse cells and 1 x10^5 cells/well for human cells) were pre-treated with CD39i (ARL 67156 trisodium salt, 200 µM, Tocris) or vehicle for 30 min and then stimulated with 1 mM ATP (Sigma) in a 96-well plate at 37 °C for 30 min. The supernatant cell culture medium was collected, and the malachite green solution was added (one-part 4.2 g ammonium molybdate dissolved in 100 mL 4 M HCl + three parts 0.045 % malachite green in H_2O). Next, optical density was measured at 650 nm. The levels of inorganic phosphate released were calculated from a parallel prepared phosphate standard curve (K_2HPO_4).

qPCR

Total RNA from $CD19^+$ B cells from the spleen was extracted using an RNeasy Mini Kit (74106, Qiagen), according to the manufacturer's directions. First-strand cDNA was synthesized from 500 µg of RNA using the high-capacity cDNA Reverse Transcription Kit (4368814, Thermo Fisher Scientific). Quantitative real-time PCR was performed using Power Syber Green PCR Master Mix TaqMan (Thermo Fisher Scientific), primers as described in the Key Resources Table and, the Viia7 Real-Time PCR system. The data were normalized to *Gapdh* values, and the fold change was analyzed using the DDCt method. The relative gene expression was expressed in arbitrary units based on the naive group, which was assigned a value of 1.

ELISA

IL-10 concentration in culture supernatants and lung tissues was determined by ELISA according to the manufacturer's instructions (R&D Systems).

ATP assay

Intracellular or extracellular ATP was detected using the ATPlite Luminescence ATP Detection Assay (PerkinElmer, Waltham, MA), according to the manufacturer's protocol. For the detection of intracellular ATP, $CD19^+$ B cells were stimulated with IL-4 (10 $ng.mL^{-1}$) at 37°C with 5% CO_2 for 6 h in the presence obligatory of a pannexin-1 channel inhibitor (carbenoxolone disodium salt, 100 µM, Sigma), and/or with 2-DG (3 mM), 3PO (30 µM), echinomycin (5 nM), oligomycin (1 µM), rotenone (2.5 µM), UK-5099 (20 µM), etomoxir (3 µM) or BPTES (10 µM). The cells were lysed to measure ATP levels 6 h later. For the detection of the extracellular ATP, we performed $CD19^+$ B cell culture stimulated with IL-4 (10 $ng.mL^{-1}$) for 6 h in the presence of a CD39 inhibitor (ARL 67156 trisodium salt, 200 µM, Tocris), and culture supernatants were collected and measured for ATP levels 6 h later. In some experiments, B cells were incubated with CBX (carbenoxolone disodium salt, 100 µM, Sigma) for measured released ATP.

Glucose uptake assay

Glucose uptake was detected using fluorescent 2-NBDG (Cayman) according to the manufacturer's protocol. B cells were plated at 1 x 10^6/well in 12-well plates and, after 18 h pre-incubation, all culture medium was removed from each well and replaced with 100 µL of culture medium without glucose in the presence of fluorescent 2-NBDG (30 µM) compounds. Plates were incubated at 37 °C with 5 % CO_2 for 30 min. The reaction was stopped by removing the incubation medium and washing the cells twice with PBS.

Metabolic Profiling

Extracellular acidification rate (ECAR) and oxygen consumption rate (OCR) were measured using the Seahorse XF96 Analyzer (Agilent Technologies) according to the manufacturer's guidelines (Agilent Seahorse XF24). Isolated $CD19^+$ B cells were stimulated with IL-4 (10 $ng.mL^{-1}$) at 37°C with 5% CO_2 for 6 h. Before analysis, 4 x 10^5 B cells were washed with XF media (for ECAR: non-buffered RPMI 1640 containing 2 mM L-glutamine and 1 mM sodium pyruvate; for OCR non-buffered RPMI 1640 containing 1 mM glucose and 1 mM sodium pyruvate)

and incubated for 30 min at 37 °C in the absence of CO_2. ECAR was measured under basal conditions and, after the addition of the following drugs: 10 mM glucose, 1 µM oligomycin, 50 mM 2DG (XF Glycolysis Stress test Kit, Agilent Technologies). OCR was measured under basal conditions and, after the addition of the following drugs: 1.5 µM Oligomycin, 1 µM FCCP, 5 µM Rotenone (XF Mito Stress test Kit, Agilent Technologies).

Re-analyzing Public Datasets

We re-analyzed single-cell transcriptomic data from the peripheral blood mononuclear cells (PBMC) of septic patients from a public dataset (Reyes et al., 2020). Basically, the samples were combined into two major groups for further comparisons, septic patients (sepsis) and non-septic patients (no sepsis). The sepsis group included samples from patients with urosepsis and patients with sepsis admitted to the medical intensive care unit, whereas the no sepsis group included samples from healthy patients and patients without sepsis admitted to the medical intensive care unit. B cells were filtered based on the authors' previous annotation for downstream analysis (Reyes et al., 2020). Specifically, the data matrices of 7970 B cells were imported to Seurat v3.1 (Stuart et al., 2019) by filtering genes expressed in at least 10 cells and more than 100 unique molecular identifiers (UMI) counts per cell. For the pre-processing step, outlier cells were filtered out based on three metrics (library size < 10000, number of expressed genes between 200 and 2000, and mitochondrial percentage expression < 5), resulting in a matrix with 13077 genes and 5104 cells. The remaining counts were normalized using the ‘LogNormalize’ method with a scale factor of 10000. The top 2,000 variable genes were then identified using the ‘vst’ method using the FindVariableFeatures function. Percent of mitochondrial genes was regressed out in the scaling step, and Principal Component Analysis (PCA) was performed using the top 2,000 variable genes with 50 dimensions. Additionally, a clustering analysis was performed on the first 7 principal components using a resolution of 0.6 followed by Uniform Manifold Approximation and Projection (UMAP), a dimensionality reduction technique for data visualization. Then, differential gene expression analysis was performed using FindAllMarkers function with default parameters to obtain a list of significant

gene markers for each cluster of cells. The plasmablast cells were identified by expression of CD39 gene counts > 0 in the RNA assay and BS3 plasmablast gene markers previously described by Reyes et al. 2020. Relative abundance of plasmablast in patients with no sepsis and with sepsis was calculated by dividing the number of plasmablasts in each group by the total number of plasmablasts. For enrichment analyses, we utilized the EnrichR tool (Chen et al., 2013) with Reactome 2016 database using plasmablast gene markers as input list.

QUANTIFICATION AND STATISTICAL ANALYSIS

Prism 8 software (GraphPad) was used for data analysis. We observed normal distribution. Survival studies were analyzed with the Mantel-Cox log-rank test, and microbial counts were calculated using the Mann–Whitney U test. Comparisons for two groups were calculated using unpaired two-tailed Student's t-tests and multiple comparisons by one-way ANOVA with Bonferroni's posthoc tests. Comparisons for the time course of CLP groups with a control group were performed using one-way ANOVA results with Dunnett posthoc tests. Correlations were analyzed with two-tailed nonparametric Spearman rank correlation tests. Differential gene expression analysis was performed using the FindAllMarkers function using the Mann–Whitney U test to obtain a list of significant gene markers for each cluster of cells with default parameters. Data are represented as means ± SEM or bacterial load as a median. Statistical significance: *$p < 0.05$; **$p < 0.01$; ***$p < 0.001$.

REFERENCE

Allard, B., Longhi, M.S., Robson, S.C., and Stagg, J. (2017). The ectonucleotidases CD39 and CD73: Novel checkpoint inhibitor targets. Immunol Rev *276*, 121-144. 10.1111/imr.12528.

Antonioli, L., Pacher, P., Vizi, E.S., and Haskó, G. (2013). CD39 and CD73 in immunity and inflammation. Trends Mol Med *19*, 355-367. 10.1016/j.molmed.2013.03.005.

Beauvais, A., Monod, M., Debeaupuis, J.P., Diaquin, M., Kobayashi, H., and Latgé, J.P. (1997). Biochemical and antigenic characterization of a new dipeptidyl-peptidase isolated from Aspergillus fumigatus. J Biol Chem *272*, 6238-6244. 10.1074/jbc.272.10.6238.

Behnsen, J., Hartmann, A., Schmaler, J., Gehrke, A., Brakhage, A.A., and Zipfel, P.F. (2008). The opportunistic human pathogenic fungus Aspergillus fumigatus evades the host complement system. Infect Immun *76*, 820-827. 10.1128/IAI.01037-07.

Benjamim, C.F., Hogaboam, C.M., Lukacs, N.W., and Kunkel, S.L. (2003). Septic mice are susceptible to pulmonary aspergillosis. Am J Pathol *163*, 2605-2617. 10.1016/S0002-9440(10)63615-2.

Berjeaud, J.M., Chevalier, S., Schlusselhuber, M., Portier, E., Loiseau, C., Aucher, W., Lesouhaitier, O., and Verdon, J. (2016). Legionella pneumophila: The Paradox of a Highly Sensitive Opportunistic Waterborne Pathogen Able to Persist in the Environment. Front Microbiol *7*, 486. 10.3389/fmicb.2016.00486.

Boomer, J.S., To, K., Chang, K.C., Takasu, O., Osborne, D.F., Walton, A.H., Bricker, T.L., Jarman, S.D., Kreisel, D., Krupnick, A.S., et al. (2011). Immunosuppression in patients who die of sepsis and multiple organ failure. JAMA *306*, 2594-2605. 10.1001/jama.2011.1829.

Borsellino, G., Kleinewietfeld, M., Di Mitri, D., Sternjak, A., Diamantini, A., Giometto, R., Höpner, S., Centonze, D., Bernardi, G., Dell'Acqua, M.L., et al. (2007). Expression of ectonucleotidase CD39 by Foxp3+ Treg cells: hydrolysis of extracellular ATP and immune suppression. Blood *110*, 1225-1232. 10.1182/blood-2006-12-064527.

Caro-Maldonado, A., Wang, R., Nichols, A.G., Kuraoka, M., Milasta, S., Sun, L.D., Gavin, A.L., Abel, E.D., Kelsoe, G., Green, D.R., and Rathmell, J.C. (2014). Metabolic reprogramming is required for antibody production that is suppressed in anergic but exaggerated in chronically BAFF-exposed B cells. J Immunol *192*, 3626-3636. 10.4049/jimmunol.1302062.

Cekic, C., Sag, D., Day, Y.J., and Linden, J. (2013). Extracellular adenosine regulates naive T cell development and peripheral maintenance. J Exp Med *210*, 2693-2706. 10.1084/jem.20130249.

Chen, E.Y., Tan, C.M., Kou, Y., Duan, Q., Wang, Z., Meirelles, G.V., Clark, N.R., and Ma'ayan, A. (2013). Enrichr: interactive and collaborative HTML5 gene list enrichment analysis tool. BMC Bioinformatics *14*, 128. 10.1186/1471-2105-14-128.

Colgan, S.P., Eltzschig, H.K., Eckle, T., and Thompson, L.F. (2006). Physiological roles for ecto-5'-nucleotidase (CD73). Purinergic Signal *2*, 351-360. 10.1007/s11302-005-5302-5.

Couper, K.N., Blount, D.G., and Riley, E.M. (2008). IL-10: the master regulator of immunity to infection. J Immunol *180*, 5771-5777. 10.4049/jimmunol.180.9.5771.

Culton, D.A., O'Conner, B.P., Conway, K.L., Diz, R., Rutan, J., Vilen, B.J., and Clarke, S.H. (2006). Early preplasma cells define a tolerance checkpoint for autoreactive B cells. J Immunol *176*, 790-802. 10.4049/jimmunol.176.2.790.

Deaglio, S., Dwyer, K.M., Gao, W., Friedman, D., Usheva, A., Erat, A., Chen, J.F., Enjyoji, K., Linden, J., Oukka, M., et al. (2007). Adenosine generation catalyzed by CD39 and CD73 expressed on regulatory T cells mediates immune suppression. J Exp Med *204*, 1257-1265. 10.1084/jem.20062512.

Dwyer, K.M., Deaglio, S., Gao, W., Friedman, D., Strom, T.B., and Robson, S.C. (2007). CD39 and control of cellular immune responses. Purinergic Signal *3*, 171-180. 10.1007/s11302-006-9050-y.

Edelstein, P.H., Weiss, W.J., and Edelstein, M.A. (2003). Activities of tigecycline (GAR-936) against Legionella pneumophila in vitro and in guinea pigs with L. pneumophila pneumonia. Antimicrob Agents Chemother *47*, 533-540. 10.1128/aac.47.2.533-540.2003.

Enjyoji, K., Sévigny, J., Lin, Y., Frenette, P.S., Christie, P.D., Esch, J.S., Imai, M., Edelberg, J.M., Rayburn, H., Lech, M., et al. (1999). Targeted disruption of cd39/ATP diphosphohydrolase results in disordered hemostasis and thromboregulation. Nat Med *5*, 1010-1017. 10.1038/12447.

Figueiró, F., Muller, L., Funk, S., Jackson, E.K., Battastini, A.M., and Whiteside, T.L. (2016). Phenotypic and functional characteristics of CD39. Oncoimmunology *5*, e1082703. 10.1080/2162402X.2015.1082703.

Fredholm, B.B., IJzerman, A.P., Jacobson, K.A., Klotz, K.N., and Linden, J. (2001). International Union of Pharmacology. XXV. Nomenclature and classification of adenosine receptors. Pharmacol Rev *53*, 527-552.

Gerdes, J., Lemke, H., Baisch, H., Wacker, H.H., Schwab, U., and Stein, H. (1984). Cell cycle analysis of a cell proliferation-associated human nuclear antigen defined by the monoclonal antibody Ki-67. J Immunol *133*, 1710-1715.

Gonçalves, A.V., Margolis, S.R., Quirino, G.F.S., Mascarenhas, D.P.A., Rauch, I., Nichols, R.D., Ansaldo, E., Fontana, M.F., Vance, R.E., and Zamboni, D.S. (2019). Gasdermin-D and Caspase-7 are the key Caspase-1/8 substrates downstream of the NAIP5/NLRC4 inflammasome required for restriction of Legionella pneumophila. PLoS Pathog *15*, e1007886. 10.1371/journal.ppat.1007886.

Guzik, T.J., Hoch, N.E., Brown, K.A., McCann, L.A., Rahman, A., Dikalov, S., Goronzy, J., Weyand, C., and Harrison, D.G. (2007). Role of the T cell in the genesis of angiotensin II induced hypertension and vascular dysfunction. J Exp Med *204*, 2449-2460. 10.1084/jem.20070657.

Hasko, G., Linden, J., Cronstein, B., and Pacher, P. (2008). Adenosine receptors: therapeutic aspects for inflammatory and immune diseases. Nat Rev Drug Discov *7*, 759-770. 10.1038/nrd2638.

Haskó, G., and Cronstein, B. (2013). Regulation of inflammation by adenosine. Front Immunol *4*, 85. 10.3389/fimmu.2013.00085.

Haskó, G., and Pacher, P. (2012). Regulation of macrophage function by adenosine. Arterioscler Thromb Vasc Biol *32*, 865-869. 10.1161/ATVBAHA.111.226852.

Jabs, C.M., Sigurdsson, G.H., and Neglen, P. (1998). Plasma levels of high-energy compounds compared with severity of illness in critically ill patients in the intensive care unit. Surgery *124*, 65-72. S0039606098001950 [pii].

Jacobson, K.A., Nikodijević, O., Padgett, W.L., Gallo-Rodriguez, C., Maillard, M., and Daly, J.W. (1993). 8-(3-Chlorostyryl)caffeine (CSC) is a selective A2-adenosine antagonist in vitro and in vivo. FEBS Lett *323*, 141-144. 10.1016/0014-5793(93)81466-d.

Kaku, H., Cheng, K.F., Al-Abed, Y., and Rothstein, T.L. (2014). A novel mechanism of B cell-mediated immune suppression through CD73 expression and adenosine production. J Immunol *193*, 5904-5913. 10.4049/jimmunol.1400336.

Lévesque, S.A., Lavoie, E.G., Lecka, J., Bigonnesse, F., and Sévigny, J. (2007). Specificity of the ecto-ATPase inhibitor ARL 67156 on human and mouse ectonucleotidases. Br J Pharmacol *152*, 141-150. 10.1038/sj.bjp.0707361.

Maliszewski, C.R., Delespesse, G.J., Schoenborn, M.A., Armitage, R.J., Fanslow, W.C., Nakajima, T., Baker, E., Sutherland, G.R., Poindexter, K., and Birks, C. (1994). The CD39 lymphoid cell activation antigen. Molecular cloning and structural characterization. J Immunol *153*, 3574-3583.

Martin, C., Leone, M., Viviand, X., Ayem, M.L., and Guieu, R. (2000). High adenosine plasma concentration as a prognostic index for outcome in patients with septic shock. Crit Care Med *28*, 3198-3202.

Mempin, R., Tran, H., Chen, C., Gong, H., Kim Ho, K., and Lu, S. (2013). Release of extracellular ATP by bacteria during growth. BMC Microbiol *13*, 301. 10.1186/1471-2180-13-301.

Nascimento, D.C., Alves-Filho, J.C., Sônego, F., Fukada, S.Y., Pereira, M.S., Benjamim, C., Zamboni, D.S., Silva, J.S., and Cunha, F.Q. (2010). Role of regulatory T cells in long-term immune dysfunction associated with severe sepsis. Crit Care Med *38*, 1718-1725. 10.1097/CCM.0b013e3181e78ad0.

Nascimento, D.C., Melo, P.H., Piñeros, A.R., Ferreira, R.G., Colón, D.F., Donate, P.B., Castanheira, F.V., Gozzi, A., Czaikoski, P.G., Niedbala, W., et al. (2017). IL-33 contributes to sepsis-induced long-term immunosuppression by expanding the regulatory T cell population. Nat Commun *8*, 14919. 10.1038/ncomms14919.

Otto, G.P., Sossdorf, M., Claus, R.A., Rödel, J., Menge, K., Reinhart, K., Bauer, M., and Riedemann, N.C. (2011). The late phase of sepsis is characterized by an increased microbiological burden and death rate. Crit Care *15*, R183. 10.1186/cc10332.

Peres, R.S., Liew, F.Y., Talbot, J., Carregaro, V., Oliveira, R.D., Almeida, S.L., França, R.F., Donate, P.B., Pinto, L.G., Ferreira, F.I., et al. (2015). Low expression of CD39 on regulatory T cells as a biomarker for resistance to methotrexate therapy in rheumatoid arthritis. Proc Natl Acad Sci U S A *112*, 2509-2514. 10.1073/pnas.1424792112.

Prescott, H.C., and Angus, D.C. (2018). Enhancing Recovery From Sepsis: A Review. JAMA *319*, 62-75. 10.1001/jama.2017.17687.

Ramakers, B.P., Riksen, N.P., van den Broek, P., Franke, B., Peters, W.H., van der Hoeven, J.G., Smits, P., and Pickkers, P. (2011). Circulating adenosine increases during human experimental endotoxemia but blockade of its receptor does not influence the immune response and subsequent organ injury. Crit Care *15*, R3. 10.1186/cc9400.

Reyes, M., Filbin, M.R., Bhattacharyya, R.P., Billman, K., Eisenhaure, T., Hung, D.T., Levy, B.D., Baron, R.M., Blainey, P.C., Goldberg, M.B., and Hacohen, N. (2020). An immune-cell signature of bacterial sepsis. Nat Med *26*, 333-340. 10.1038/s41591-020-0752-4.

Rittirsch, D., Huber-Lang, M.S., Flierl, M.A., and Ward, P.A. (2009). Immunodesign of experimental sepsis by cecal ligation and puncture. Nat Protoc *4*, 31-36. 10.1038/nprot.2008.214.

Robson, S.C., Sévigny, J., and Zimmermann, H. (2006). The E-NTPDase family of ectonucleotidases: Structure function relationships and pathophysiological significance. Purinergic Signal *2*, 409-430. 10.1007/s11302-006-9003-5.

Rosser, E.C., and Mauri, C. (2015). Regulatory B cells: origin, phenotype, and function. Immunity *42*, 607-612. 10.1016/j.immuni.2015.04.005.

Rosser, E.C., Piper, C.J.M., Matei, D.E., Blair, P.A., Rendeiro, A.F., Orford, M., Alber, D.G., Krausgruber, T., Catalan, D., Klein, N., et al. (2020). Microbiota-Derived Metabolites Suppress Arthritis by Amplifying Aryl-Hydrocarbon Receptor Activation in Regulatory B Cells. Cell Metab *31*, 837-851.e810. 10.1016/j.cmet.2020.03.003.

Sattler, S., Ling, G.S., Xu, D., Hussaarts, L., Romaine, A., Zhao, H., Fossati-Jimack, L., Malik, T., Cook, H.T., Botto, M., et al. (2014). IL-10-producing regulatory B cells induced by IL-33 (Breg(IL-33)) effectively attenuate mucosal inflammatory responses in the gut. J Autoimmun *50*, 107-122. 10.1016/j.jaut.2014.01.032.

Saze, Z., Schuler, P.J., Hong, C.S., Cheng, D., Jackson, E.K., and Whiteside, T.L. (2013). Adenosine production by human B cells and B cell-mediated suppression of activated T cells. Blood *122*, 9-18. 10.1182/blood-2013-02-482406.

Singer, M., Deutschman, C.S., Seymour, C.W., Shankar-Hari, M., Annane, D., Bauer, M., Bellomo, R., Bernard, G.R., Chiche, J.D., Coopersmith, C.M., et al. (2016). The Third International Consensus Definitions for Sepsis and Septic Shock (Sepsis-3). JAMA *315*, 801-810. 10.1001/jama.2016.0287.

Solomkin, J.S., Mazuski, J.E., Bradley, J.S., Rodvold, K.A., Goldstein, E.J., Baron, E.J., O'Neill, P.J., Chow, A.W., Dellinger, E.P., Eachempati, S.R., et al. (2010). Diagnosis and management of complicated intra-abdominal infection in adults and children: guidelines by the Surgical Infection Society and the Infectious Diseases Society of America. Surg Infect (Larchmt) *11*, 79-109. 10.1089/sur.2009.9930.

Steinhauser, M.L., Hogaboam, C.M., Kunkel, S.L., Lukacs, N.W., Strieter, R.M., and Standiford, T.J. (1999). IL-10 is a major mediator of sepsis-induced impairment in lung antibacterial host defense. J Immunol *162*, 392-399.

Stuart, T., Butler, A., Hoffman, P., Hafemeister, C., Papalexi, E., Mauck, W.M., Hao, Y., Stoeckius, M., Smibert, P., and Satija, R. (2019). Comprehensive Integration of Single-Cell Data. Cell *177*, 1888-1902.e1821. 10.1016/j.cell.2019.05.031.

Tsui, C., Martinez-Martin, N., Gaya, M., Maldonado, P., Llorian, M., Legrave, N.M., Rossi, M., MacRae, J.I., Cameron, A.J., Parker, P.J., et al. (2018). Protein Kinase C-β Dictates B Cell Fate by Regulating Mitochondrial Remodeling, Metabolic Reprogramming, and Heme Biosynthesis. Immunity *48*, 1144-1159.e1145. 10.1016/j.immuni.2018.04.031.

Tung, J.W., Mrazek, M.D., Yang, Y., and Herzenberg, L.A. (2006). Phenotypically distinct B cell development pathways map to the three B cell lineages in the mouse. Proc Natl Acad Sci U S A *103*, 6293-6298. 10.1073/pnas.0511305103.

Venet, F., and Monneret, G. (2018). Advances in the understanding and treatment of sepsis-induced immunosuppression. Nat Rev Nephrol *14*, 121-137. 10.1038/nrneph.2017.165.

Veras, F.P., Peres, R.S., Saraiva, A.L., Pinto, L.G., Louzada-Junior, P., Cunha, T.M., Paschoal, J.A., Cunha, F.Q., and Alves-Filho, J.C. (2015). Fructose 1,6-bisphosphate, a high-energy intermediate of glycolysis, attenuates experimental arthritis by activating anti-inflammatory adenosinergic pathway. Sci Rep *5*, 15171. 10.1038/srep15171.

Wang, T., Derhovanessian, A., De Cruz, S., Belperio, J.A., Deng, J.C., and Hoo, G.S. (2014). Subsequent infections in survivors of sepsis: epidemiology and outcomes. J Intensive Care Med *29*, 87-95. 10.1177/0885066612467162.

Waters, L.R., Ahsan, F.M., Wolf, D.M., Shirihai, O., and Teitell, M.A. (2018). Initial B Cell Activation Induces Metabolic Reprogramming and Mitochondrial Remodeling. iScience *5*, 99-109. 10.1016/j.isci.2018.07.005.

Yoshizaki, A., Miyagaki, T., DiLillo, D.J., Matsushita, T., Horikawa, M., Kountikov, E.I., Spolski, R., Poe, J.C., Leonard, W.J., and Tedder, T.F. (2012). Regulatory B cells control T-cell autoimmunity through IL-21-dependent cognate interactions. Nature *491*, 264-268. 10.1038/nature11501.

Zamboni, D.S., Kobayashi, K.S., Kohlsdorf, T., Ogura, Y., Long, E.M., Vance, R.E., Kuida, K., Mariathasan, S., Dixit, V.M., Flavell, R.A., et al. (2006). The Birc1e cytosolic pattern-recognition receptor contributes to the detection and control of Legionella pneumophila infection. Nat Immunol *7*, 318-325. 10.1038/ni1305.